



Akademie věd České republiky
Ústav teorie informace a automatizace

Academy of Sciences of the Czech Republic
Institute of Information Theory and Automation

RESEARCH REPORT

RADOMÍR VÁVRA, JIŘÍ FILIP, PETR SOMOL

A Comparison of Adaptive Sampling and Interpolation of 2D BRDF Subspaces

No. 2339

22 December 2013

ÚTIA AV ČR, Pod Vodárenskou věží 4, 182 08 Prague, Czech Republic

E-mail: vavra@utia.cas.cz

Tel: +420 266 052 365

Fax: +420 284 683 031

A Comparison of Adaptive Sampling and Interpolation of 2D BRDF Subspaces

Radomír Vávra, Jiří Filip, Petr Somol

Abstract

This report comprises overview of interpolation and sampling methods of Bidirectional Reflectance Distribution Function (BRDF). We analyzed 2D BRDF subspaces of eleven materials. We compared performance of five interpolation methods, three different sampling patterns, and compared twelve adaptive sampling strategies. Finally, based on knowledge of entire data we estimated sub-optimal sampling patterns and as a reference compared them with other tested sampling approaches.

Real-world appearance of spatially homogeneous materials can be represented by means of a bidirectional reflectance distribution function (BRDF) introduced by Nicodemus et al. [8]. $BRDF(\lambda, \theta_i, \theta_v, \varphi_i, \varphi_v)$ is a five-dimensional function of light wavelength or color spectrum λ , illumination direction $\omega_i = [\theta_i, \varphi_i]$ and view direction $\omega_v = [\theta_v, \varphi_v]$ as shown in Fig. 1.

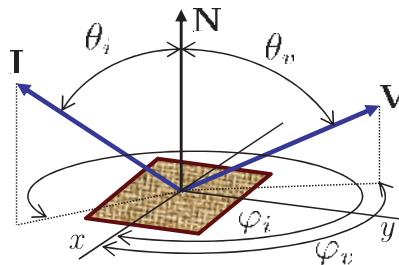


Figure 1: BRDF parameterization within a local coordinate system.

Given the fact that any ground truth dense anisotropic BRDF measurements of sufficient quality are not available so far (apart from measurement of *fabric002* material [2]), we used high-quality fits of Kurt analytical BRDF model [6] as our reference. We selected ten materials, four of them measured by Ngan et al. [7]; fitted in [6], and the remaining materials come from our own measurements. All of the materials are anisotropic and include fabrics, brushed aluminum, and raw wood. The BRDFs of measured *fabric002* material and the fits of ten materials are shown in Fig. 2

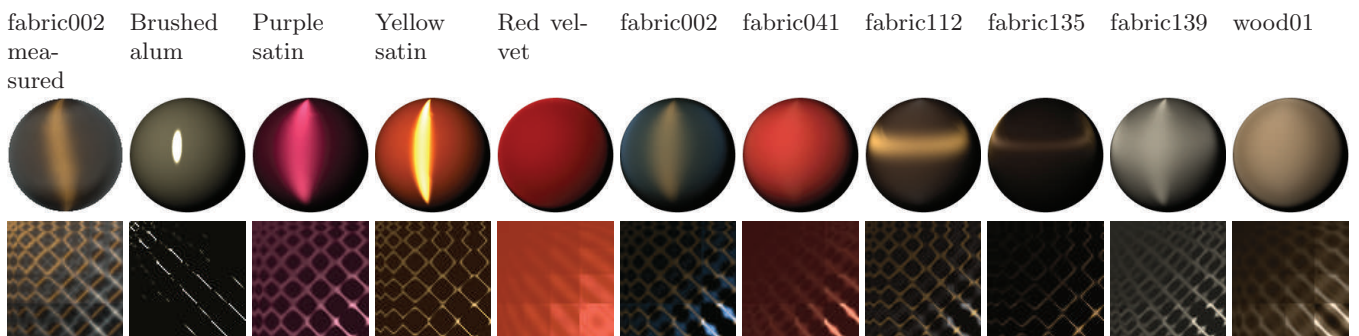


Figure 2: Eleven tested materials. One measured and ten reconstructed using 1 or 2 lobes of Kurt BRDF model [6].

In this comparison we have used two-dimensional BRDF subspaces of eleven materials. Division of BRDF into the subspaces is shown in Fig. 3-(a). On horizontal axis varies azimuth of view direction φ_v with step 0.5° and on vertical axis varies azimuth of illumination direction φ_i with step 0.5° .

For our experiments we selected subspace for fixed view and illumination elevations $\theta_v = \theta_i = 75^\circ$ (see Fig. 3-(b)) where the BRDF function exhibits the highest visual contrast with narrow specular and anisotropic highlights. The subspaces of the tested materials are depicted as color images in Fig. 4. These images were used as our reference data in this report.

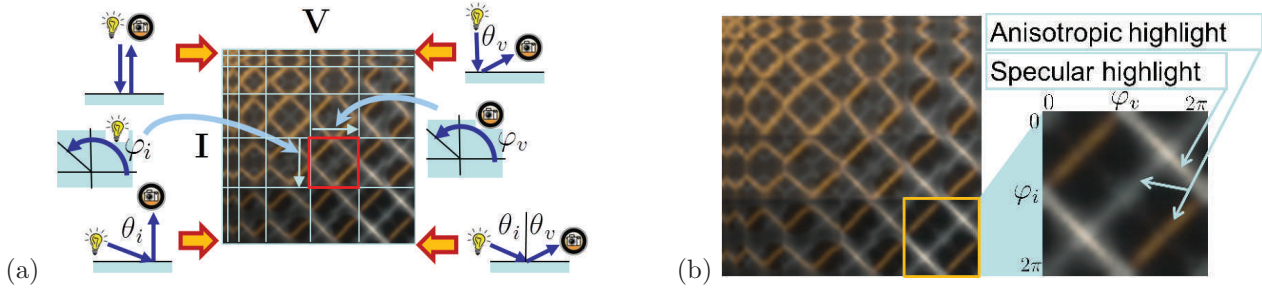


Figure 3: BRDF its subdivision into azimuthal subspaces (a) and description of azimuthal subspace for elevation angles $\theta_i/\theta_v = 75^\circ/75^\circ$ (b) used as reference data in this report.

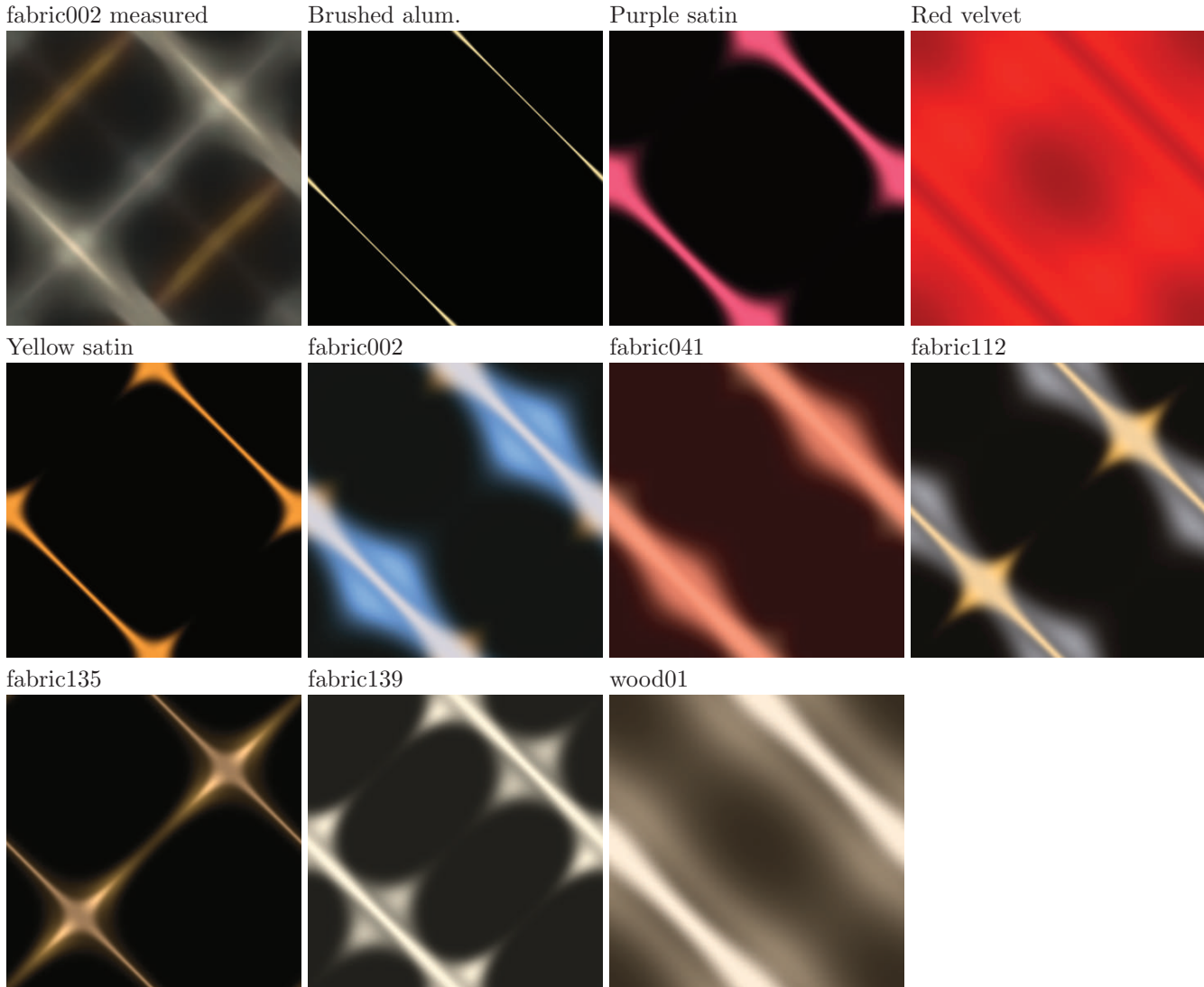


Figure 4: BRDF subspaces of the eleven tested materials.

As azimuth angles of view and illumination vary with step 0.5° ground truth images consists of $M = 720 \times 720 = 518400$ samples. Such a high sample count is far away from possibilities of any measurement device measuring one sample at a time. So to reconstruct images of original resolution we use only $N = 576$ samples which can be measured in reasonable time and we interpolate them to reach original resolution. Distribution of this samples can be static regardless of measured material properties or it can be adaptive with respect to material properties.

Report Overview In Section 2 we compare various interpolation techniques reconstructing images of original resolution 720×720 samples from samples placed in static uniform grid of resolution 24×24 samples. Section 3 shows influence of different static sampling patterns to quality of resulted interpolated images. Section 4 presents twelve strategies of material sampling with respect to its properties. In Section 5 we deal with techniques searching

for optimal sampling patterns of given materials. Section 6 concludes the paper.

1 Methodology

Here we describe how a performance of individual interpolation sampling techniques is evaluated. Resulted images can be compared with each other and with ground truth image using direct pixel-wise comparison. Also difference images \mathbf{D} between ground truth \mathbf{I}_{gt} and interpolated \mathbf{I}_{ip} images can be helpful in quality evaluation. Each pixel (x, y) of difference image \mathbf{D} was computed as $\mathbf{D}(x, y) = 255 - 10 \times |\mathbf{I}_{gt}(x, y) - \mathbf{I}_{ip}(x, y)|$. It means the darker pixel in difference image the bigger difference between ground truth and interpolated image.

Further, several image difference metrics were used. The first one is ΔE which uses Euclidean distance in perceptually uniform CIE 1976 (L^*, a^*, b^*) color space

$$\Delta E = \sqrt{(L_{gt} - L_{ip})^2 + (a_{gt} - a_{ip})^2 + (b_{gt} - b_{ip})^2},$$

where L_{gt}, a_{gt}, b_{gt} are luminance and chromaticity components of the ground truth image and L_{ip}, a_{ip}, b_{ip} are luminance and chromaticity components of the interpolated image. Root mean square error (RMS) is defined as

$$RMS = \sqrt{\frac{\sum_{i=1}^M \sum_{\lambda=RGB} (I_{gt}(i, \lambda) - I_{ip}(i, \lambda))^2}{N_{gt} * 3}}.$$

Maximal difference (MD) is not metric but has significant informational value. It is distance of two maximally distant pixels

$$MD = \max_{i=1}^M \max_{\lambda=RGB} |I_{gt}(i, \lambda) - I_{ip}(i, \lambda)|.$$

The higher value of these metrics the bigger reconstruction error (\uparrow).

Peak signal-to-noise ration (PSNR) is directly computed from RMS as

$$PSNR = 20 \cdot \log_{10} \frac{255^2}{RMS}.$$

Structural similarity (SSIM) index is a measure between two images converted into levels of gray [10]. For this two last metrics hold the higher value the better reconstruction (\downarrow).

Results in a rest of the paper are organized in Figures as follows. First row contains names of methods used. Next row often contains sampling pattens. Then there are the interpolated images \mathbf{I}_{ip} and the difference images \mathbf{D} . Below the difference images is row with $\uparrow \Delta E / RMS / MD$ and then row with $\downarrow PSNR / SSIM$ metrics. The last row might contain interpolation times or times consumed by adaptive sampling strategies. Bold numbers denote the best performance in given metric/time for current material.

2 Comparison of Various Interpolation Techniques

In this section we compare quality of five interpolation techniques. The first interpolation method is pull-push algorithm [5] based on image pyramid, the second is barycentric interpolation [1] based on linear interpolation between three closest samples. The third method uses radial basis functions (RBF) with gaussian kernels [9], the fourth is based on Kriging [9], and the fifth uses radial basis functions with thin plate splines [9].

The results are organized as follows. First column is reserved for ground truth image and sampling mask showing in which pixels was ground truth image sampled (the mask is regular grid of resolution 24×24 samples and is same across all the materials). In the other columns are the results itself. The first row contains names of interpolation techniques used. In the second row are interpolated images and in the third are difference images. The fourth row contains values of image difference metrics $\uparrow \Delta E / RMS / MD$ for which hold the lower value the better quality. In the next row are $\downarrow PSNR / SSIM$. The last row contains achieved interpolation times.

Summary Although for few materials is the best reconstruction quality achieved by very fast pull-push or barycentric algorithms the best quality of the others is achieved by method based on radial basis functions with gaussian kernels (RBF). Reconstruction quality using Kriging and TPS algorithms is close behind RBF but their processing times are much longer. On the other hand these algorithms perform well even for unevenly distributed samples while RBF does not.

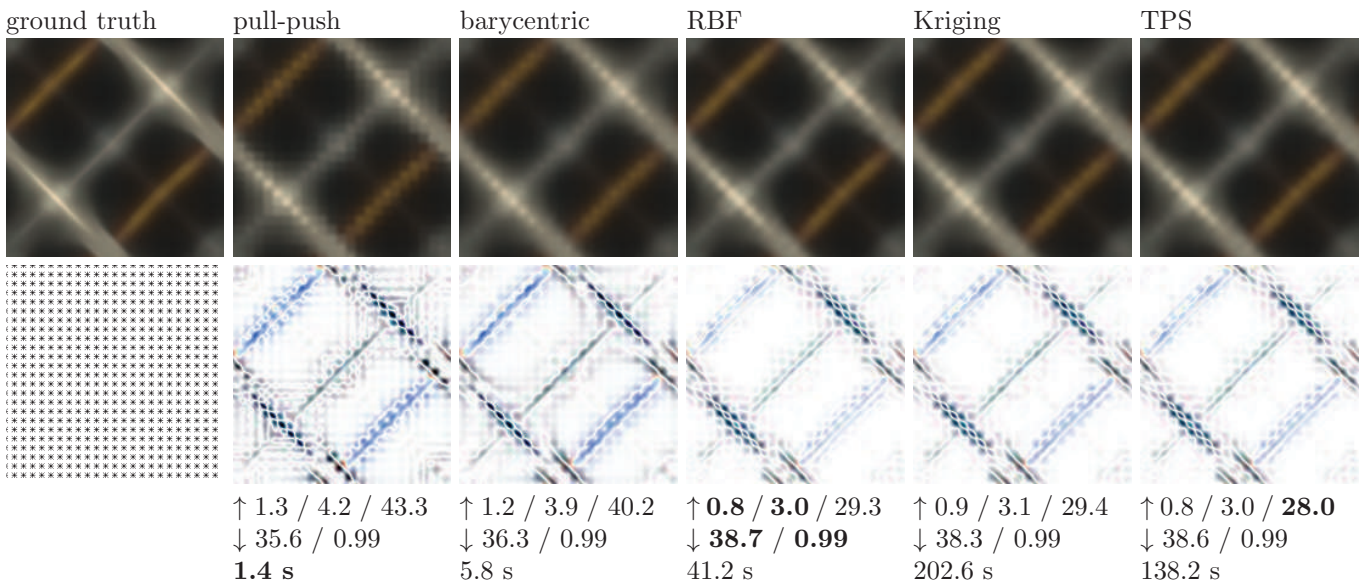


Figure 5: Material fabric002 measured. Sample count $N = 576$. Metrics are ΔE , RMS, MD and PSNR, SSIM.

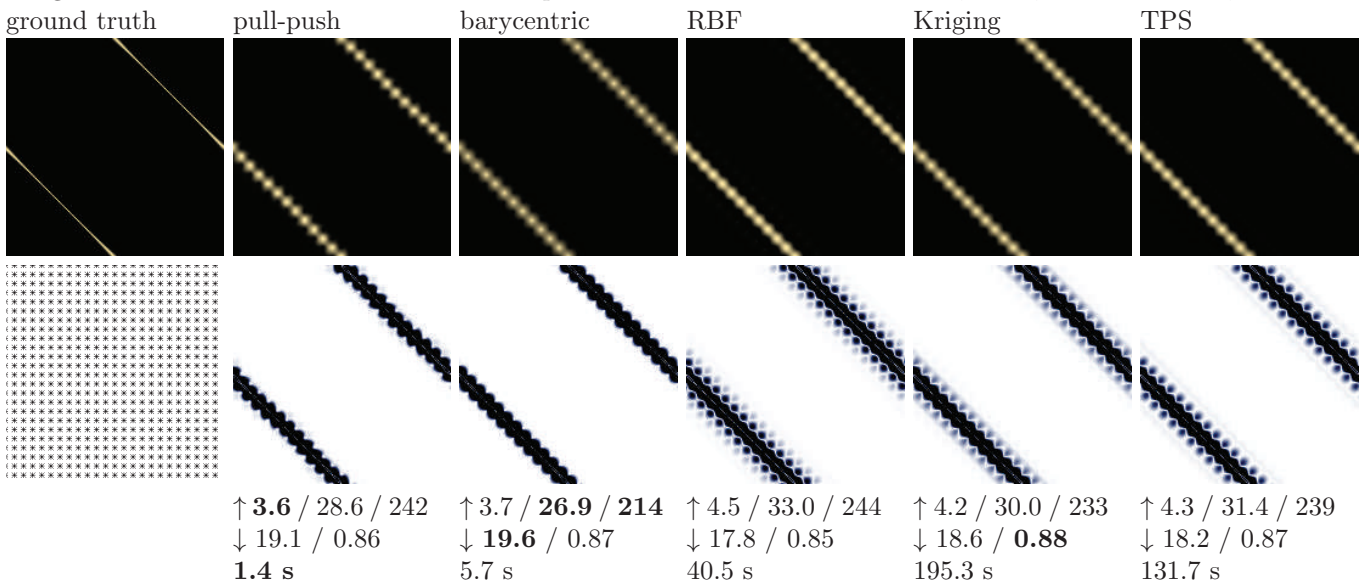


Figure 6: Material Brushed alum. Sample count $N = 576$. Metrics are ΔE , RMS, MD and PSNR, SSIM.

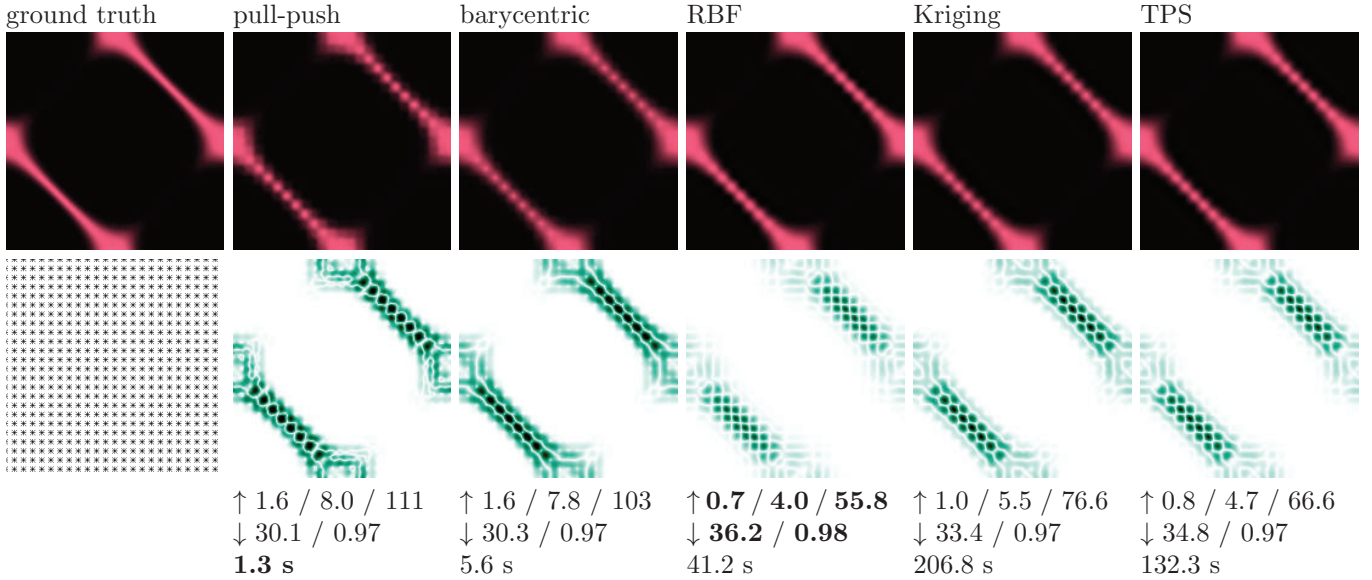


Figure 7: Material Purple satin. Sample count $N = 576$. Metrics are ΔE , RMS, MD and PSNR, SSIM.

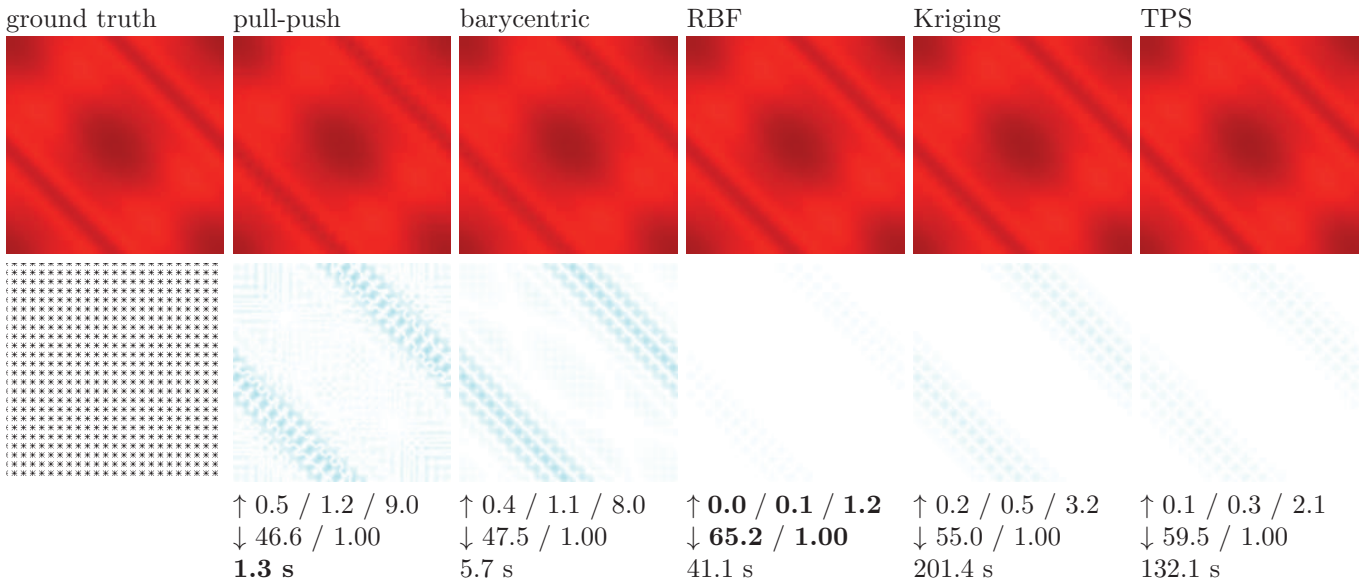


Figure 8: Material Red velvet. Sample count $N = 576$. Metrics are ΔE , RMS, MD and PSNR, SSIM.

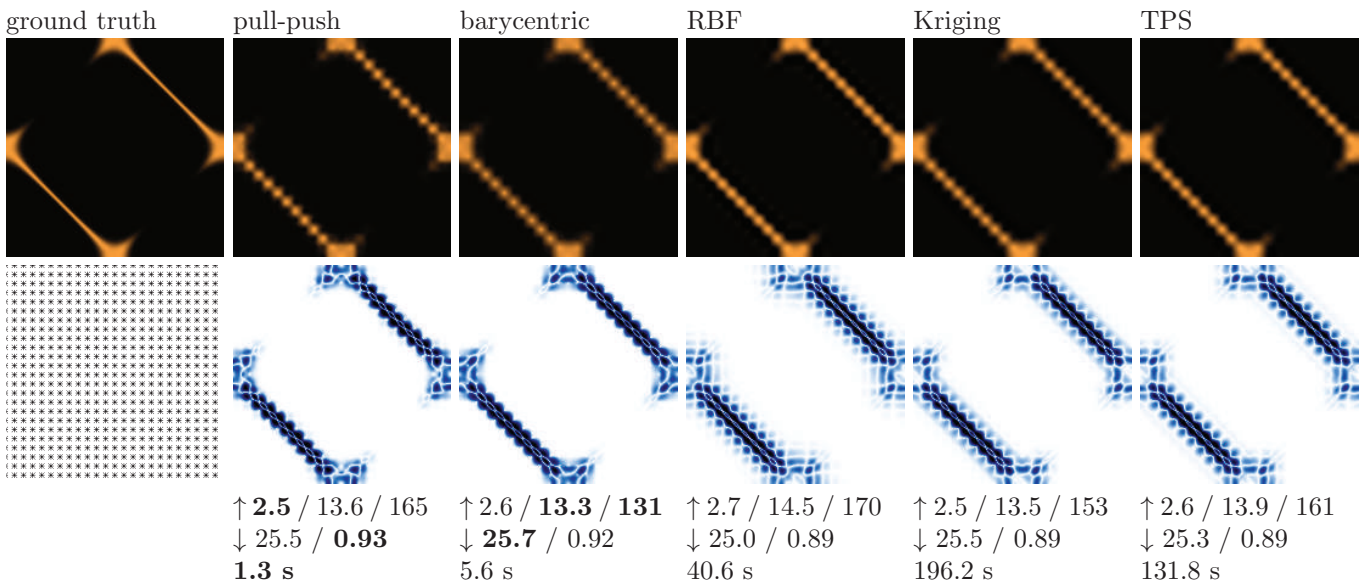


Figure 9: Material Yellow satin. Sample count $N = 576$. Metrics are ΔE , RMS, MD and PSNR, SSIM.

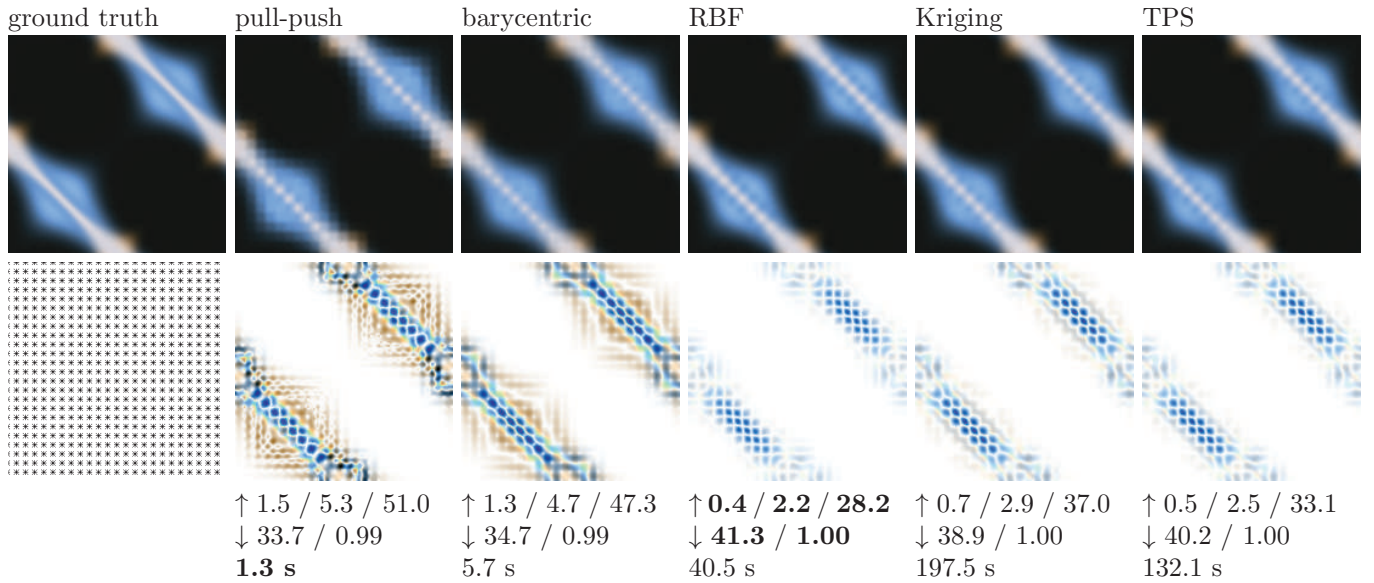


Figure 10: Material fabric002. Sample count $N = 576$. Metrics are ΔE , RMS, MD and PSNR, SSIM.

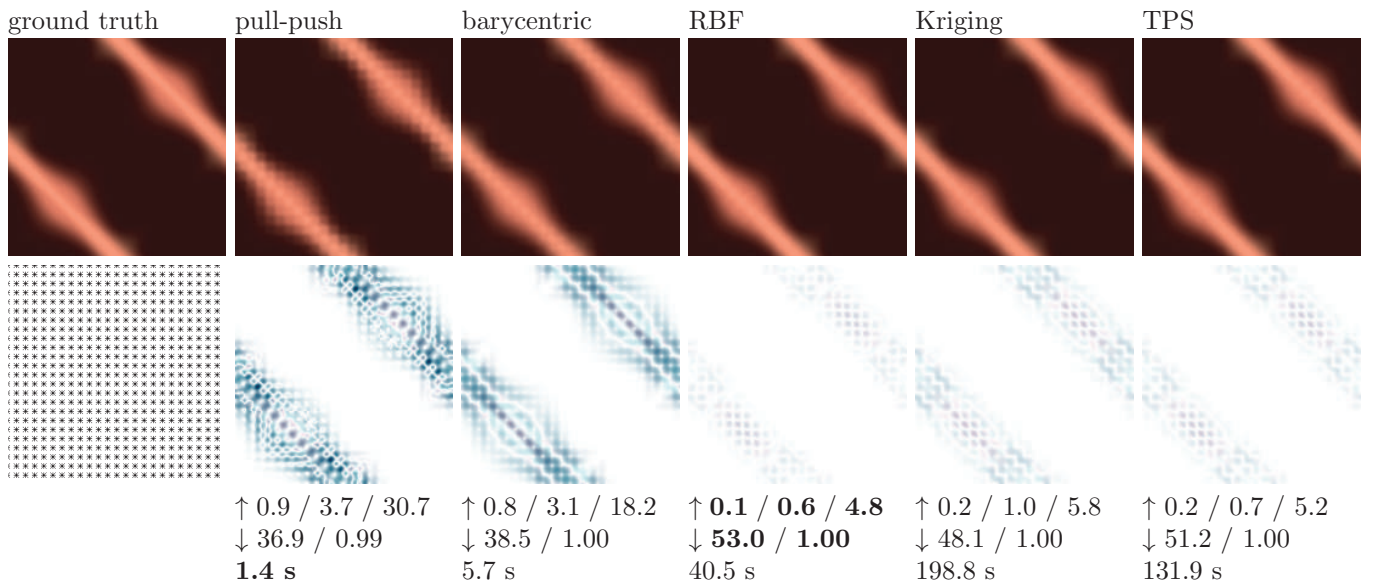


Figure 11: Material fabric041. Sample count $N = 576$. Metrics are ΔE , RMS, MD and PSNR, SSIM.

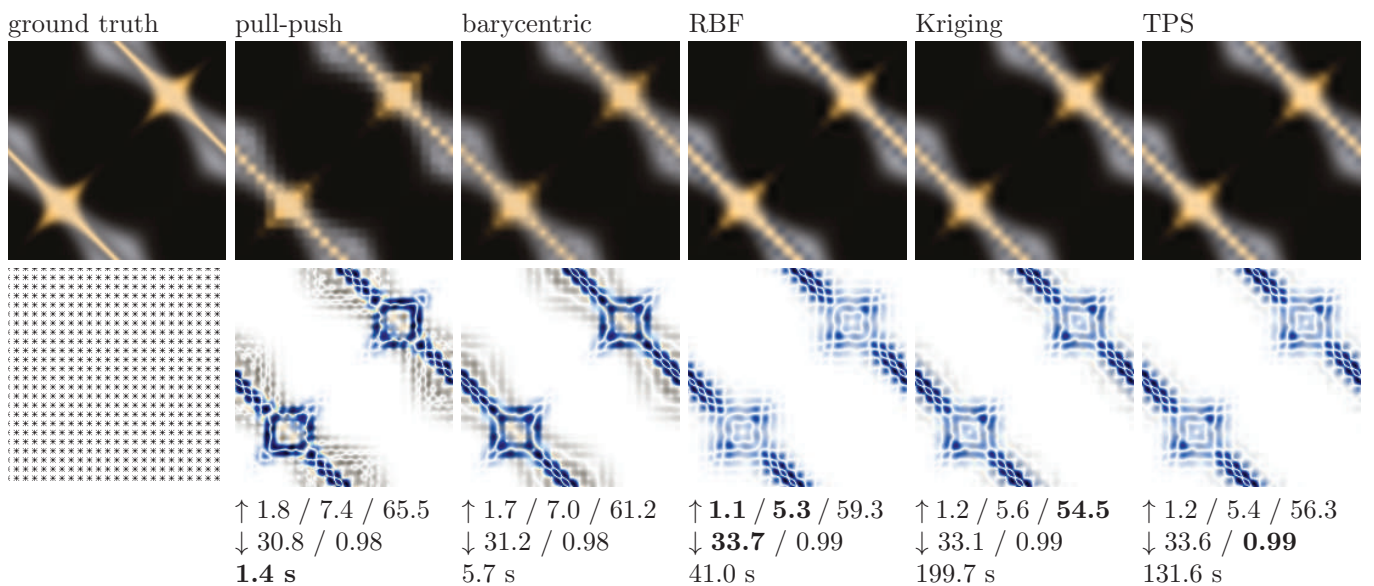


Figure 12: Material fabric112. Sample count $N = 576$. Metrics are ΔE , RMS, MD and PSNR, SSIM.

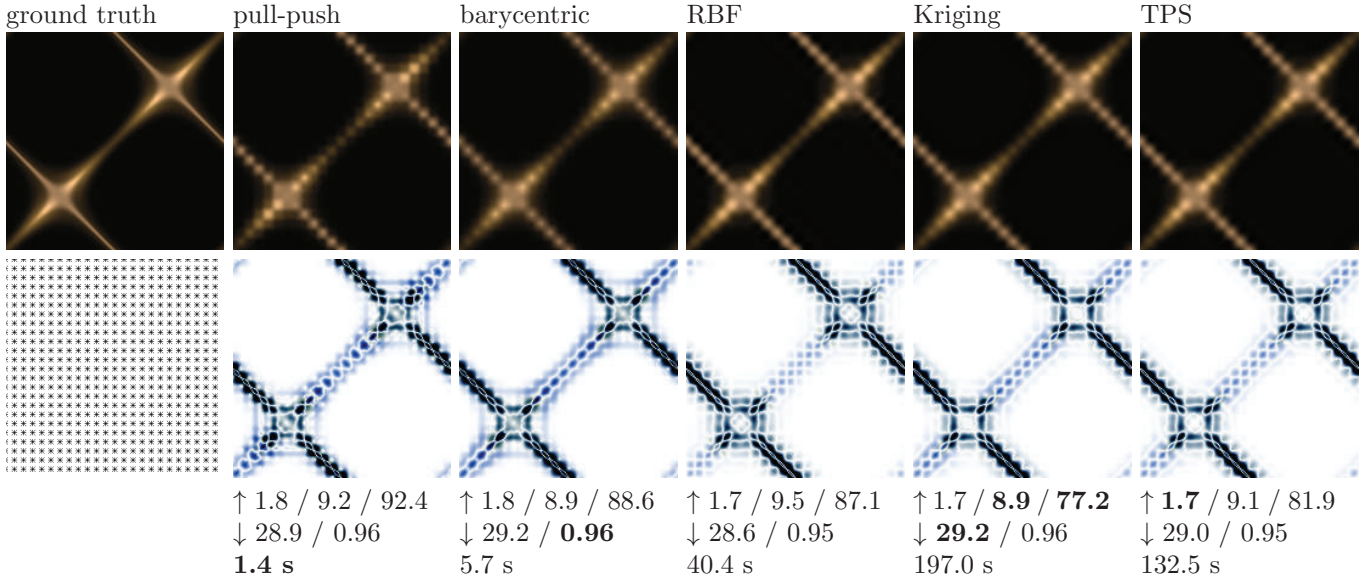


Figure 13: Material fabric135. Sample count $N = 576$. Metrics are ΔE , RMS, MD and PSNR, SSIM.

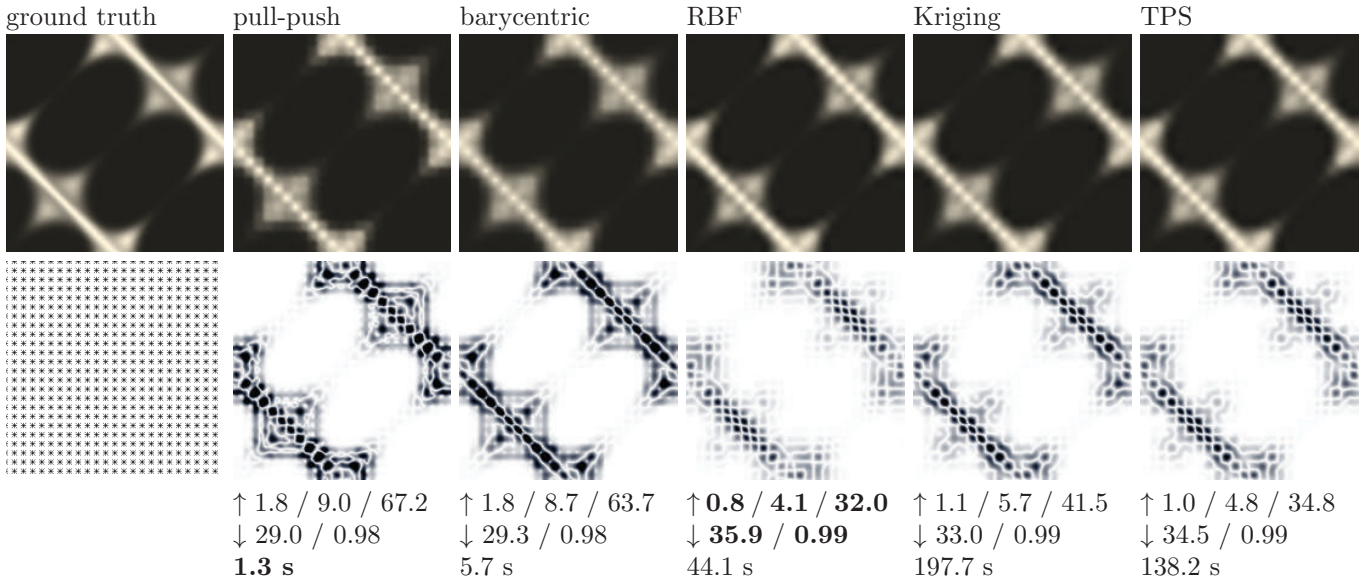


Figure 14: Material fabric139. Sample count $N = 576$. Metrics are ΔE , RMS, MD and PSNR, SSIM.

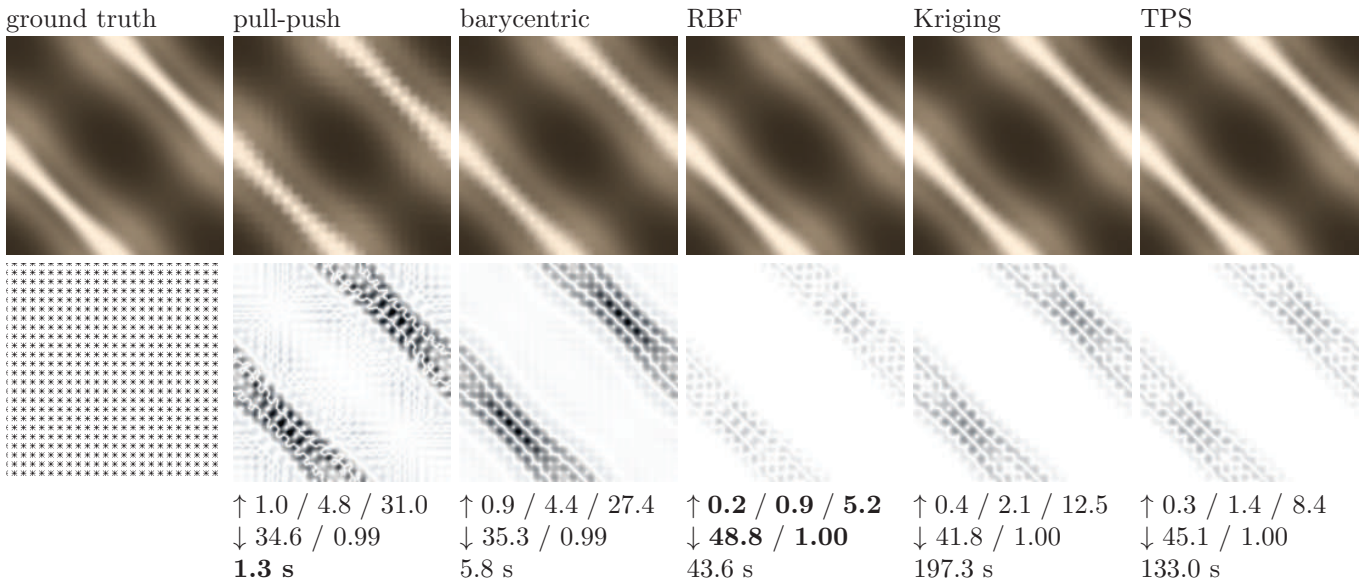


Figure 15: Material wood01 151. Sample count $N = 576$. Metrics are ΔE , RMS, MD and PSNR, SSIM.

3 Comparison of Different Static Sampling Patterns

This section compares influence of static sampling patterns on the reconstruction quality. As in section 2 interpolation based on radial basis functions with gaussian kernels (RBF) performs the best we used only this method in this Section. Sampling Patterns used are depicted in Fig. 16. The first is sampling in uniform grid with resolution 24×24 already used in Section 2. The second one is similar though the pattern is rotated for 45° and 578 samples are used in this pattern so that pattern is uniform. In the last pattern are samples distributed pseudo-randomly generated by Hammersley generator. We tested five different pseudo-random patterns and then we chosen the one that performs better than the others.

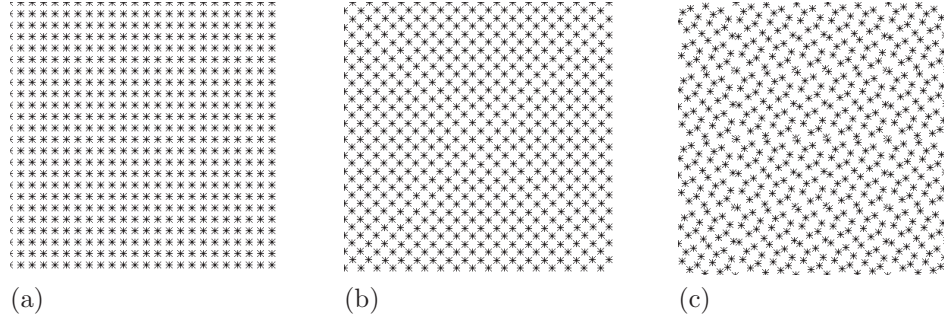


Figure 16: (a) 576 static uniform samples, (b) 578 static uniform samples 45° rotated, (c) 576 static random samples.

The results are presented in form of figures where left three columns contain one material while right three columns contain another one. Below reconstructed images are difference images ten times multiplied, values of $\uparrow \Delta E / RMS / MD$ and values of $\downarrow PSNR / SSIM$ (see Sec. 1).

Summary Static uniform grid reaches always the best results in terms of metrics used. On the other hand samples in pattern rotated for 45° achieve better visual quality. Pseudo-random sampling does not work well.

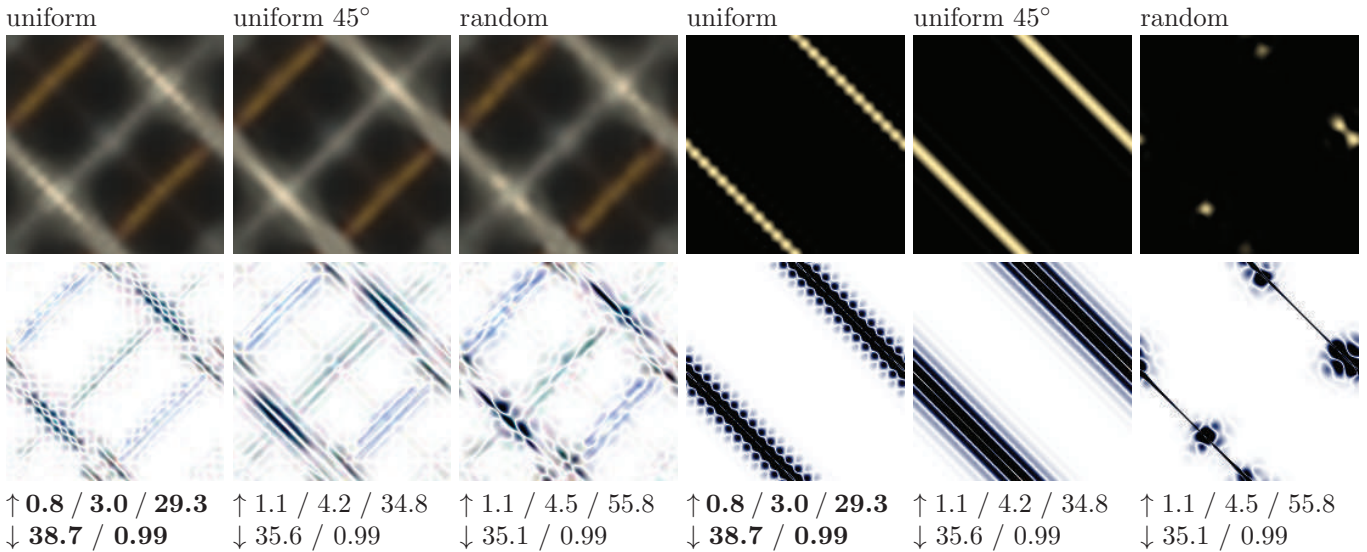


Figure 17: Material fabric002 measured and Brushed alum. Sample count $N = 576$ or $N = 578$.

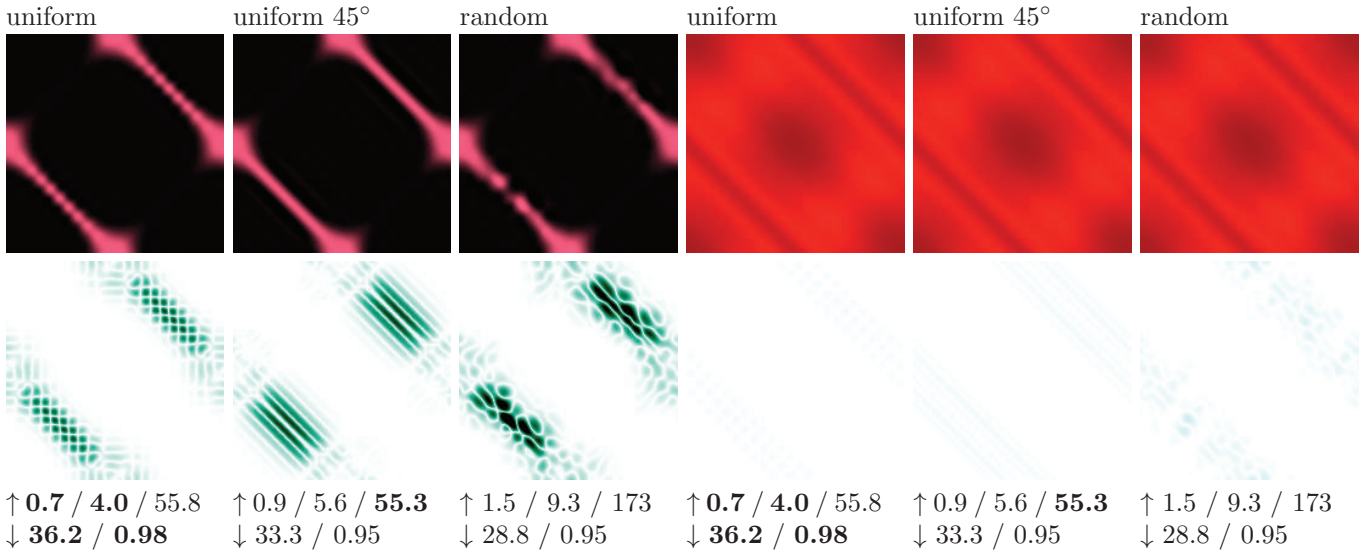


Figure 18: Material Purple satin and Red velvet. Sample count $N = 576$ or $N = 578$.

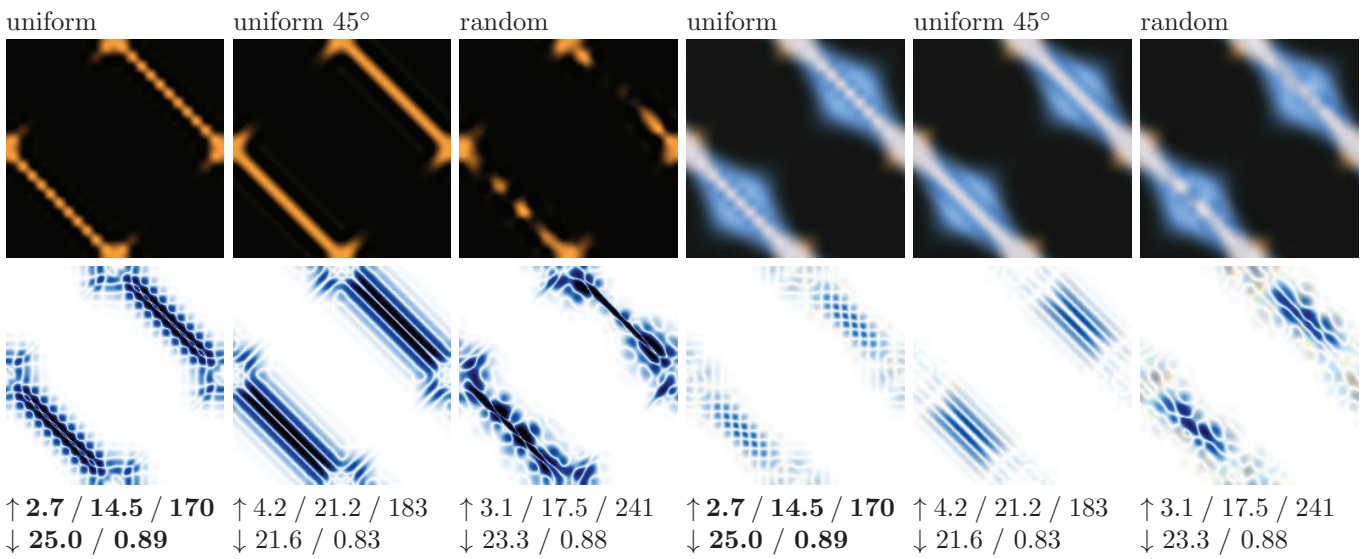


Figure 19: Material Yellow satin and fabric002. Sample count $N = 576$ or $N = 578$.

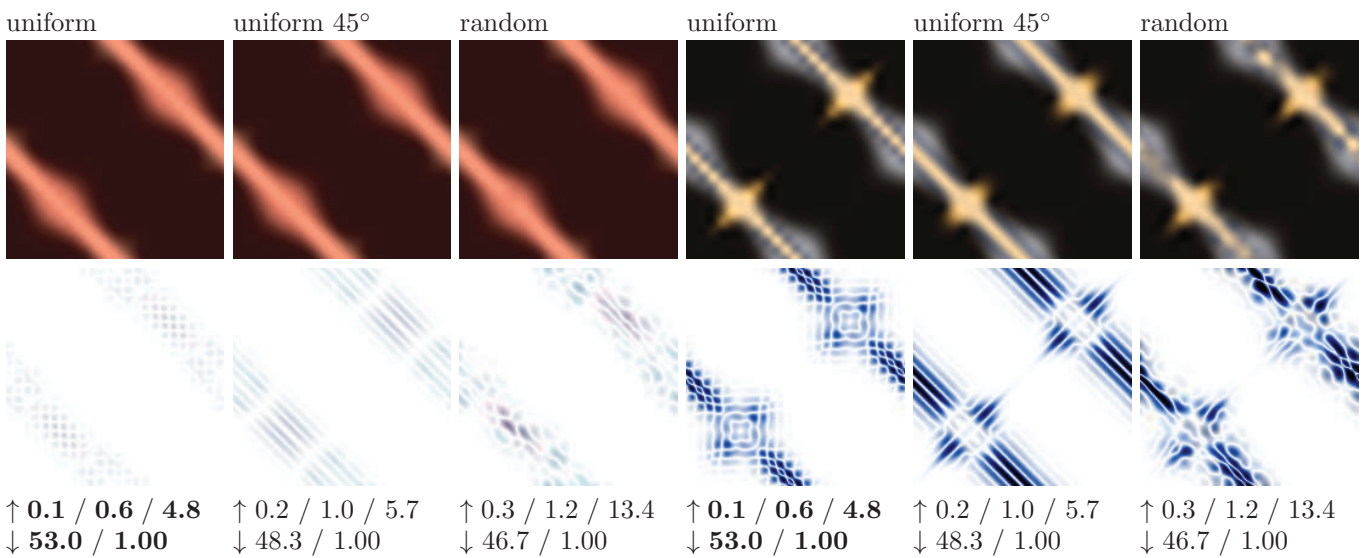


Figure 20: Material fabric041 and fabric112. Sample count $N = 576$ or $N = 578$.

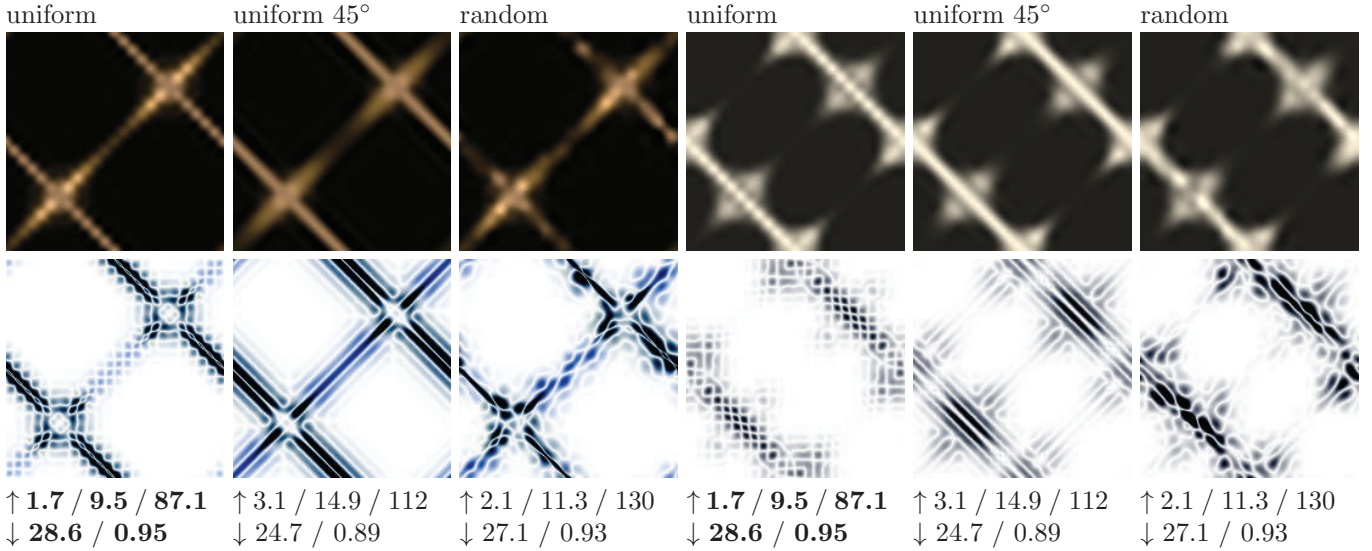


Figure 21: Material fabric135 and fabric139. Sample count $N = 576$ or $N = 578$.

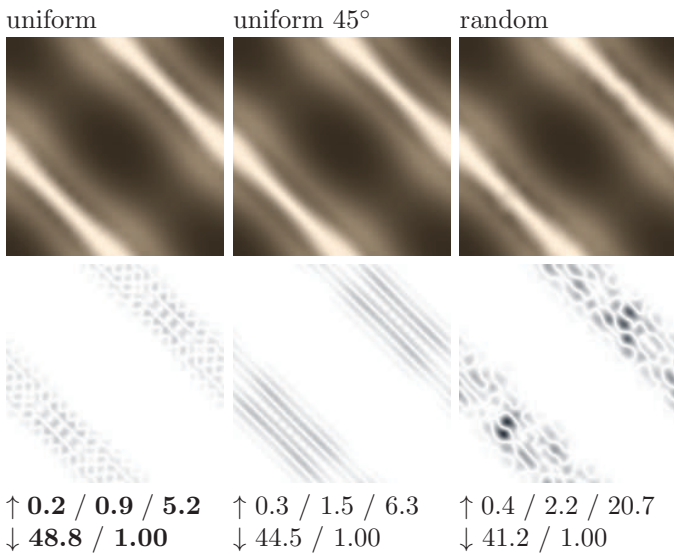


Figure 22: Material wood01 151. Sample count $N = 576$ or $N = 578$.

4 Comparison of Adaptive Sampling Approaches

In this section we present results of adaptive sampling methods. As according to Section 3 the distribution of samples in regular grid is superior to other distributions these methods start with uniform distribution of samples in regular grid with resolution $12 \times 12 = 144$ samples. New samples are placed according to rules summed in Tab. 1 and final count of samples is 576. In strategies 1 to 3 several samples are placed in each iteration. In strategies 4 to 12 only one sample is placed in each iteration of our algorithm.

First step of all the strategies starts with computation of Delaunay triangulation of already measured samples. For strategies 1 to 9 is computed cross-validation error of each vertex. The error in each vertex is computed using next three steps. First, the vertex is leaved out and the triangulation is recomputed. Second, barycentric interpolation of values in vertices of new triangle into which the vertex belongs is computed. Third, the error is computed as Euclidean distance of interpolated and actual value in the vertex.

For strategies 10 to 12 dissimilarity in each vertex is computed as maximal Euclidean distance of values of current and neighborhood vertex across all neighbors of the vertex. Neighbor of the vertex is each vertex connected with it by edge in triangulation.

In the next step the one element (vertex, edge, triangle) is chosen. In strategies 1 to 3 is chosen vertex with maximal cross-validation error and new samples are added into center of all adjacent edges of this vertex (strategy 1), into circumcenters of all adjacent triangles (strategy 2) or into centroids of all adjacent triangles (strategy 3). The circumcenter of a triangle is the point with equal distance from all triangles vertices. The point may not be inside the triangle. The centroid of a triangle is the point in intersection of the three medians of the triangle. Each median connects one vertex of triangle with the center of the opposite side. The centroid is always inside the triangle.

Table 1: Decision rules where to place new sample(s) for various adaptive sampling strategies.

<i>error measure</i>	<i>decision control element</i>	<i>edge</i>	<i>circumcenter</i>	<i>centroid</i>
cross-validation	vertex with maximal error	strategy 1	strategy 2	strategy 3
	vertex with maximal error and his neighbor(s) with maximal error	strategy 4	strategy 5	strategy 6
	element with maximal sum of errors	strategy 7	strategy 8	strategy 9
dissimilarity	element with maximal sum of errors	strategy 10	strategy 11	strategy 12

In strategies 4 to 6 is chosen vertex with maximal cross-validation error too and then is selected adjacent element (edge, triangle) whose sum of cross-validation errors in its vertices is maximal. New sample is added into center of resulting edge (strategy 4) or in circumcenter (strategy 5) or centroid (strategy 6) of resulting triangle.

In strategies 7 to 9 is directly chosen element (edge, triangle) with maximal sum of cross-validation errors in its vertices and new sample is added into center of resulting edge (strategy 7) or into circumcenter (strategy 8) or centroid (strategy 9) of resulting triangle.

Similarly in strategies 10 to 12 is chosen element (edge, triangle) with maximal sum of dissimilarity in its vertices and new sample is added into center of resulting edge (strategy 10) or into circumcenter (strategy 11) or centroid (strategy 12) of resulting triangle. Strategy 11 was originally published in [4] though in our implementation only one sample in each iteration is added.

Below interpolated images of all strategies are presented times adaptive sampling techniques needed to reach 576 samples. These times are lower for strategies 1 to 3 as they add several samples in each iteration and for strategies 10 to 12 as they do not need to recompute triangulation in cross-validation error computation step. It would be possible to implement iterative Delaunay triangulation and significantly lower computation times for strategies 1 to 9.

Summary The most competitive strategies are number 2 and 11. Also strategies 1, 3, 10 and 12 perform often well. The most likely conclusion is that strategies 10 to 12 work well as dissimilarity error measure is better than cross-validation error measure and strategies 1 to 3 work well as they place several samples in each iteration. Also it is clearly better place new sample into circumcenter of a triangle than into centroid or center of edge as the new sample is equally far from triangle vertices. Even if the new sample is not inside the triangle into which circumcenter was placed due to Delaunay triangulation it cannot be too close to any other sample. Summarizing these observations up the best strategy should place new sample into circumcenter of a triangle, it should use dissimilarity error measure and it should place several samples in each iteration of the algorithm. This is exactly the method already published in [4]. New experiments should be performed to find optimal number of samples added in each iteration of the algorithm.



Figure 23: Material fabric002 measured. Strategies start with 144 samples and finish with 576 samples.

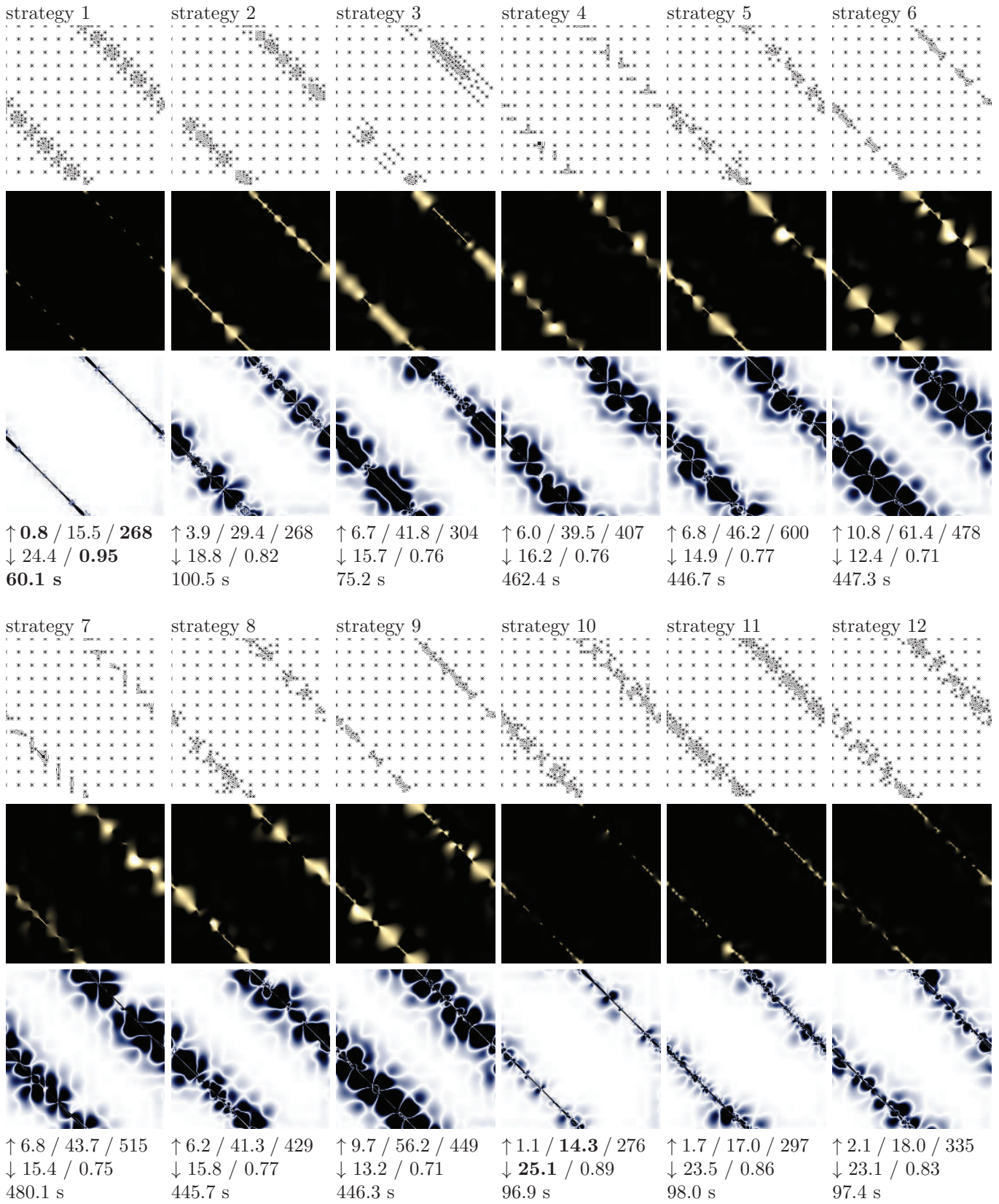


Figure 24: Material Brushed alum. Strategies start with 144 samples and finish with 576 samples.

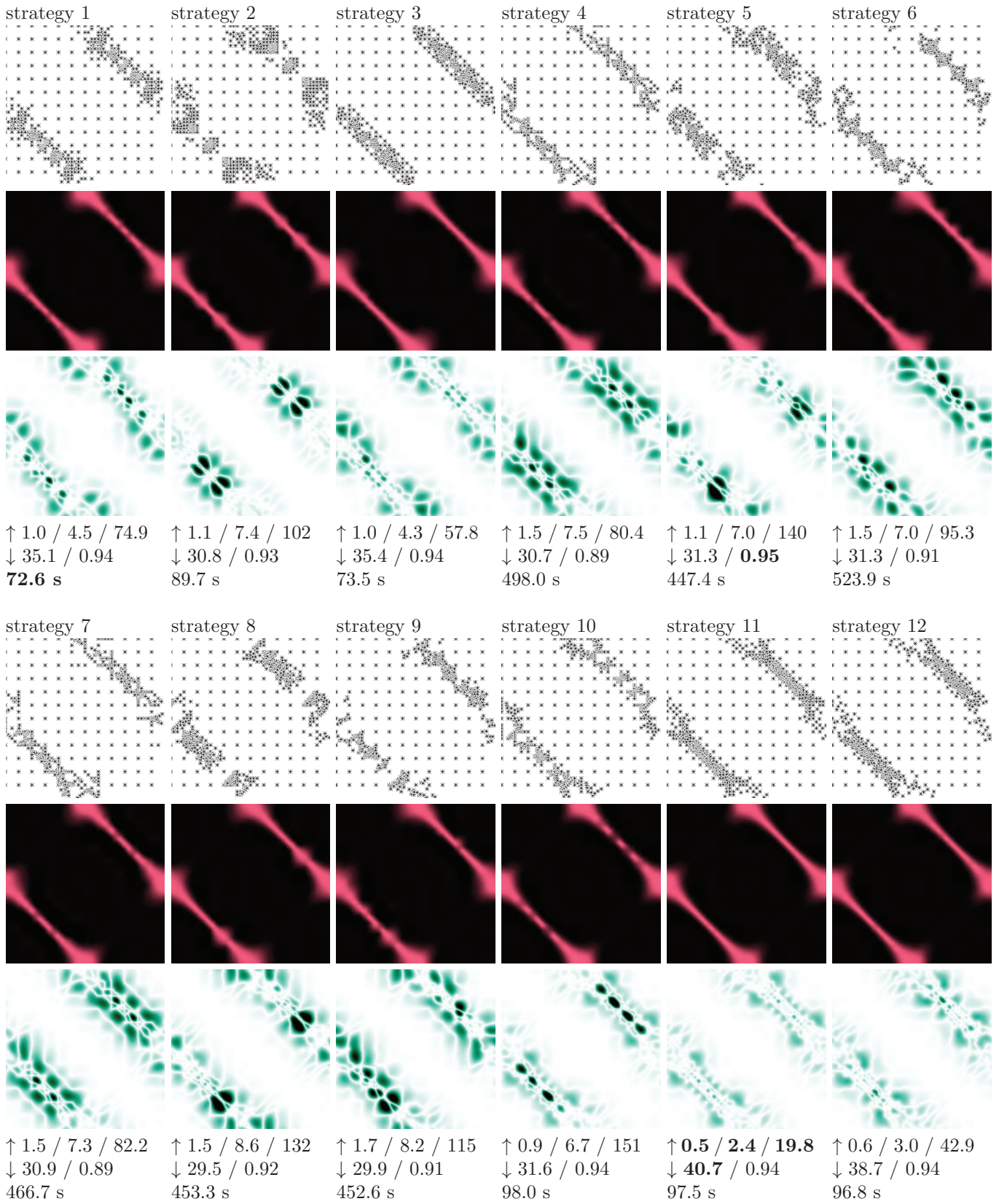


Figure 25: Material Purple satin. Strategies start with 144 samples and finish with 576 samples.

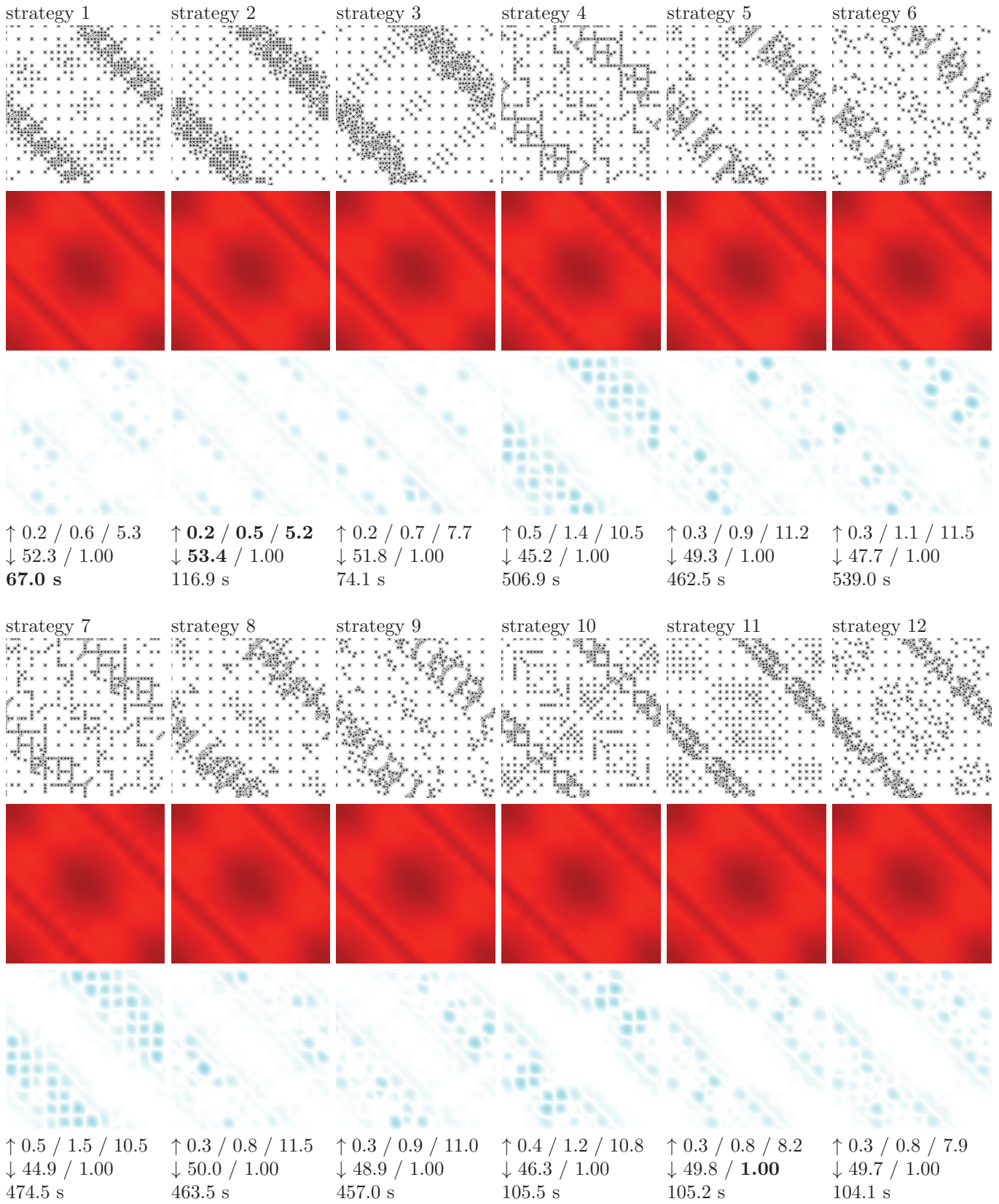


Figure 26: Material Red velvet. Strategies start with 144 samples and finish with 576 samples.

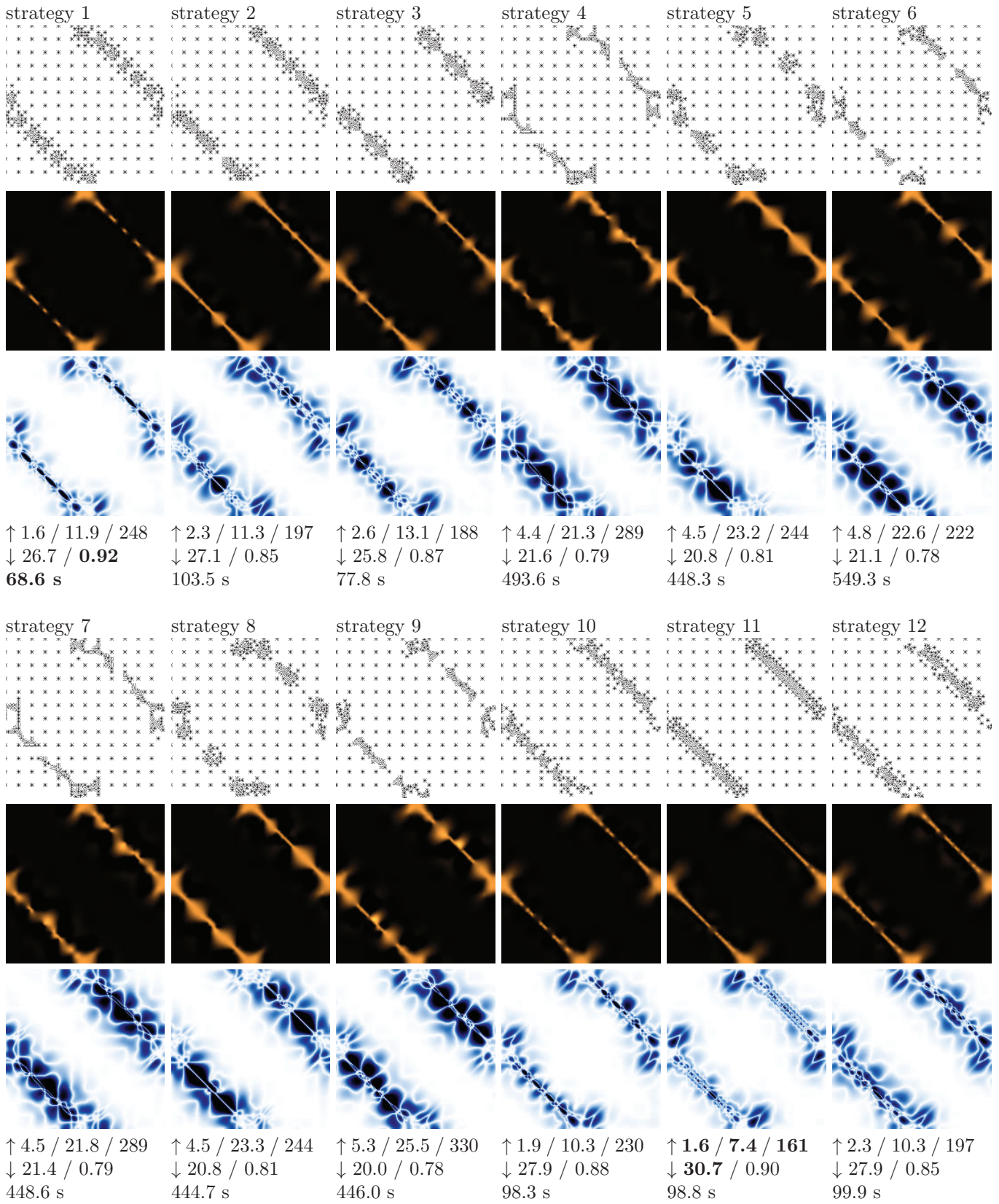


Figure 27: Material Yellow satin. Strategies start with 144 samples and finish with 576 samples.

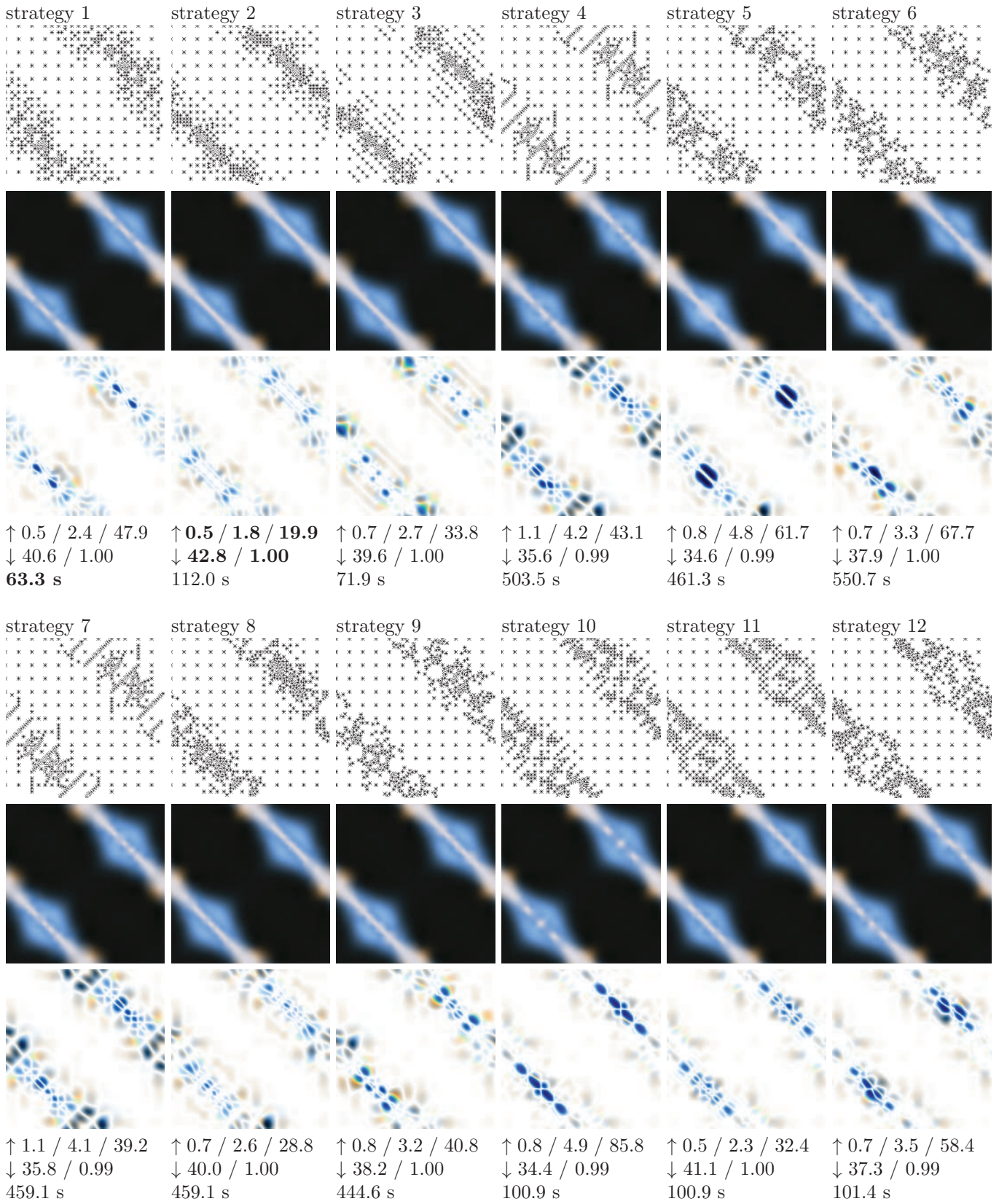


Figure 28: Material fabric002. Strategies start with 144 samples and finish with 576 samples.

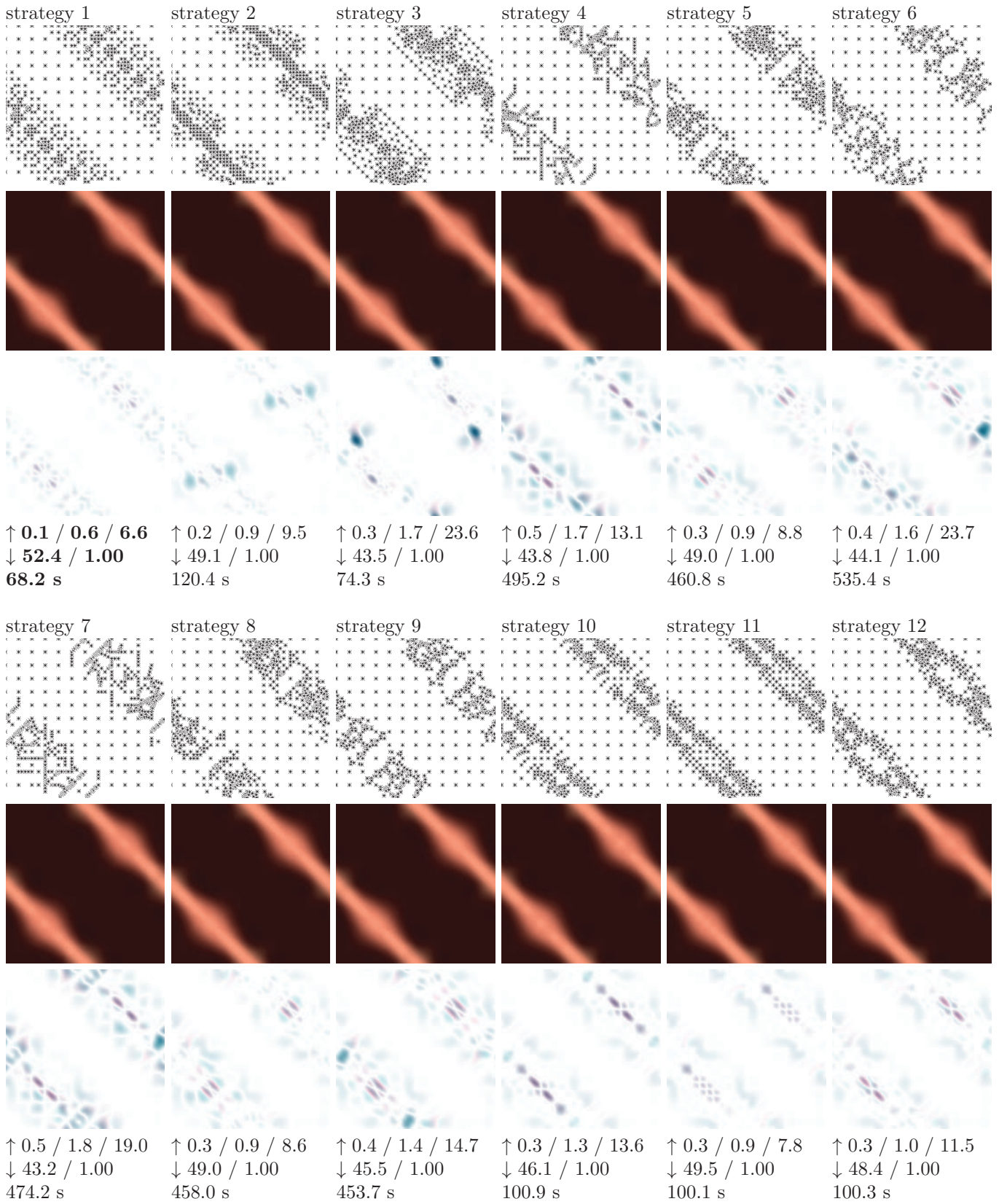


Figure 29: Material fabric041. Strategies start with 144 samples and finish with 576 samples.

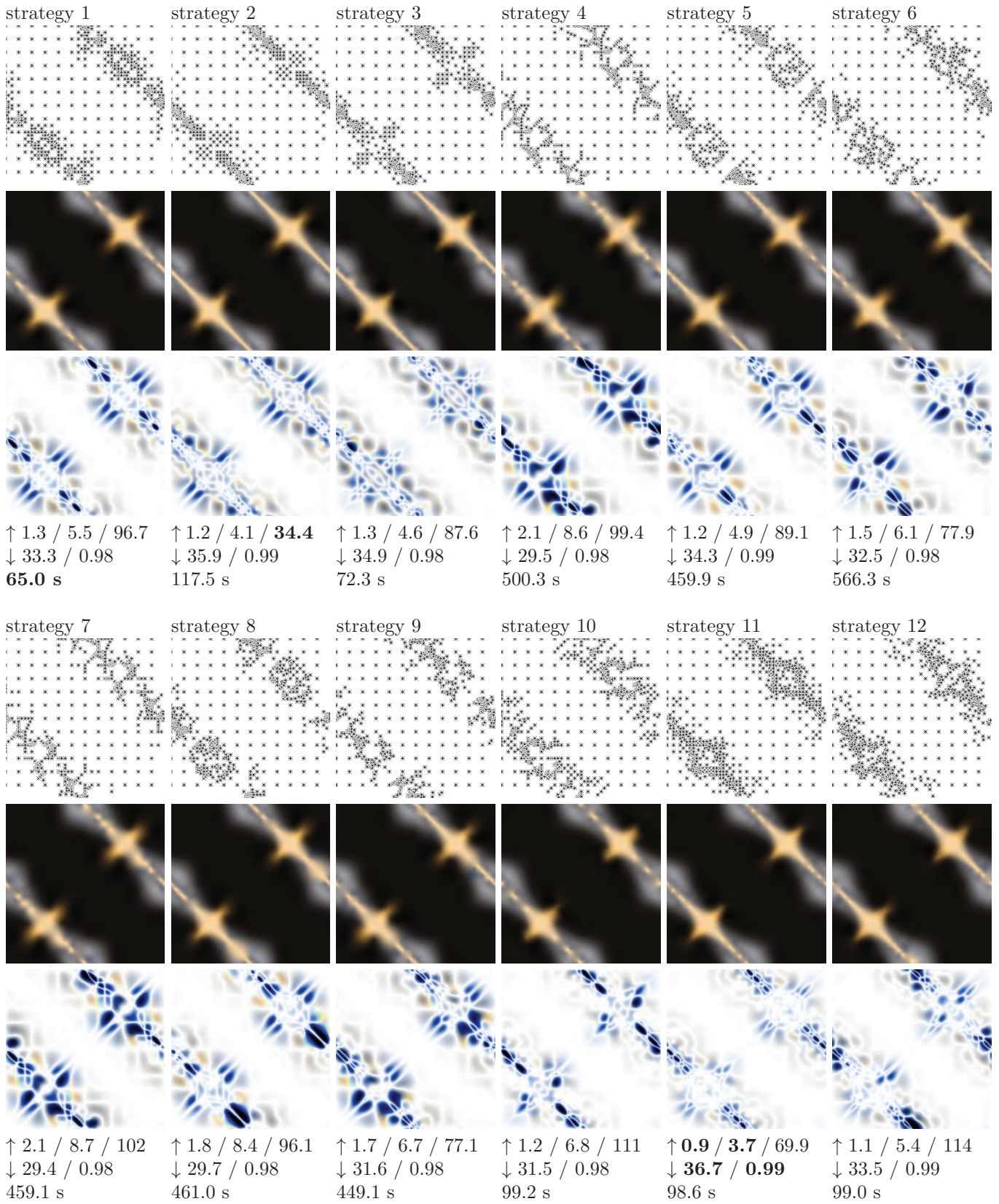


Figure 30: Material fabric112. Strategies start with 144 samples and finish with 576 samples.

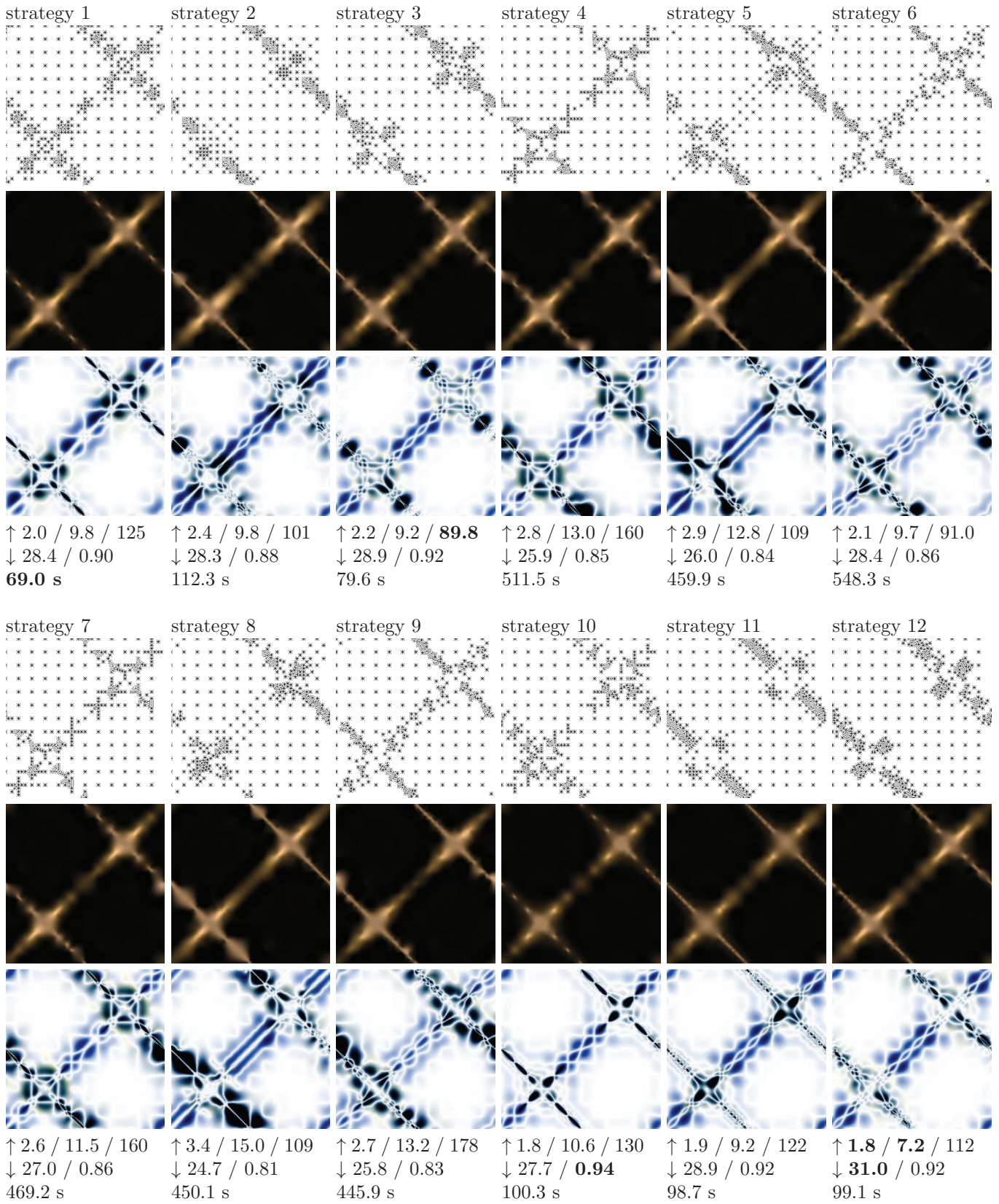


Figure 31: Material fabric135. Strategies start with 144 samples and finish with 576 samples.

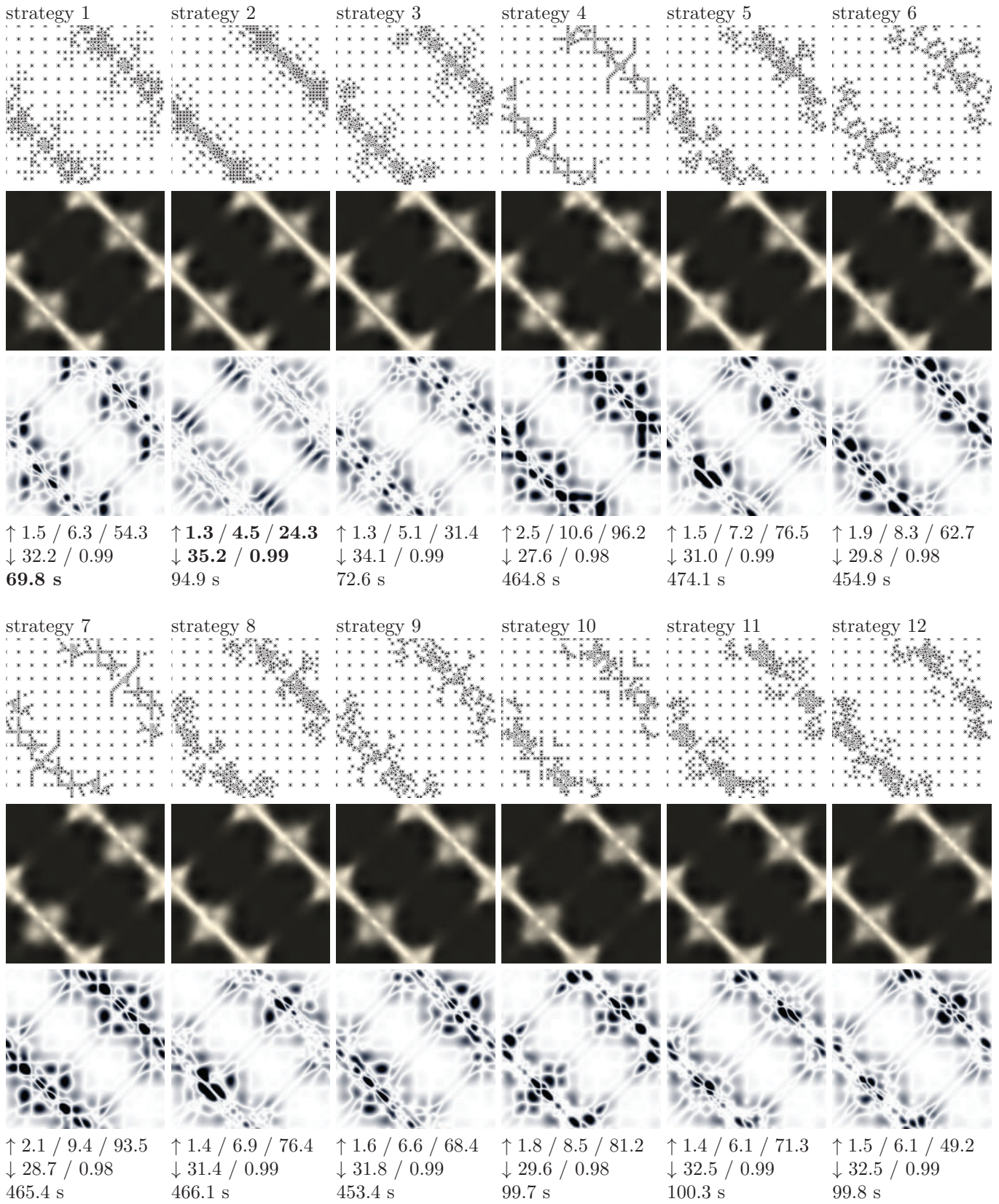


Figure 32: Material fabric139. Strategies start with 144 samples and finish with 576 samples.

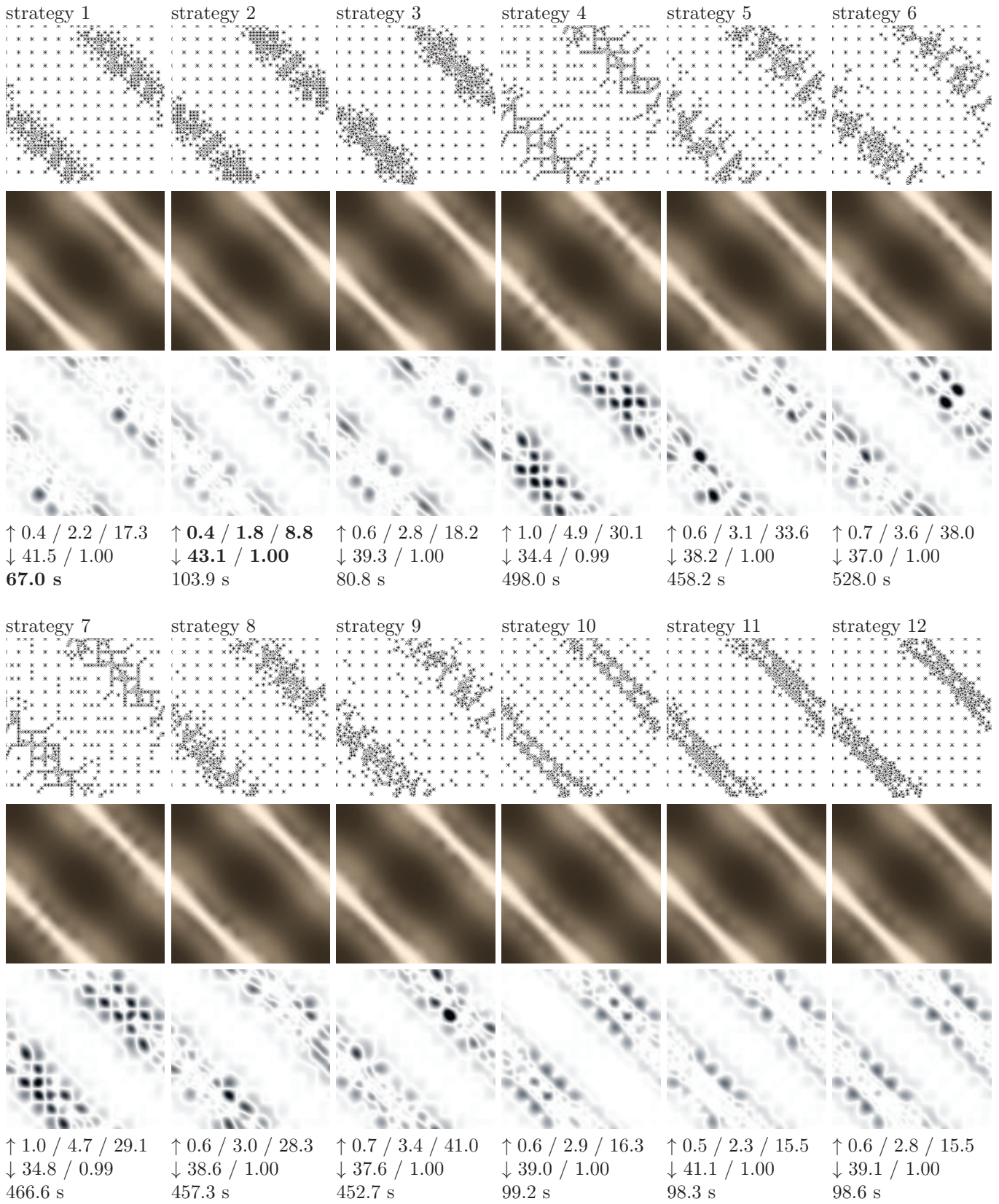


Figure 33: Material wood01 151. Strategies start with 144 samples and finish with 576 samples.

5 Comparison of Techniques Looking for Optimal Sample Placements

In contrast with approaches proposed in Section 4 now we assume knowledge of all $M = 720 \times 720 = 518400$ sample values and we are looking for optimal placement of $N = 576$ samples from which can be original image reconstructed as accurately as possible.

First approach we tried is Floyd-Steinberg dithering [3]. The algorithm achieves dithering by distributing the residual quantization error of a pixel onto its neighboring pixels. Figure 34 shows that algorithm does not work well for our purposes.

Another approach is based on iterative removing of samples with minimal cross-validation error. The algorithm consists of two steps. In the first one a cross-validation error in each remaining sample is evaluated. The error is computed as Euclidean distance between actual and interpolated value in the sample. Interpolation is done by Kriging interpolation method using 20 samples closest to the current one. Lets call these 20 closest samples as supporting samples. In the second step samples with minimal cross-validation error are removed until we should remove sample whose supporting sample was already removed. Then the first step has to be performed again. The algorithm stops when required number of remaining samples is reached.

During testing the algorithm we have noticed that sometimes the algorithm performs better on sample grids with lower resolution. So we present results for five different resolutions. In the first one samples vary with step 0.5° so there are $M_{0.5} = 720 \times 720 = 518400$ samples. In the second one samples vary with step 1° and $M_1 = 360 \times 360 = 129600$. Other steps are 2° , 4° , and 8° and sample counts are $M_2 = 180 \times 180 = 32400$, $M_4 = 90 \times 90 = 8100$, and $M_8 = 45 \times 45 = 2025$.

Summary The algorithm based on iterative removing of samples reaches good results. It presents sampling patterns as one would expected. On the other hand the fact that using lower resolution results can perform better means that the algorithm is not optimal. We believe there exists another algorithm with polynomial execution time that can produce better results.

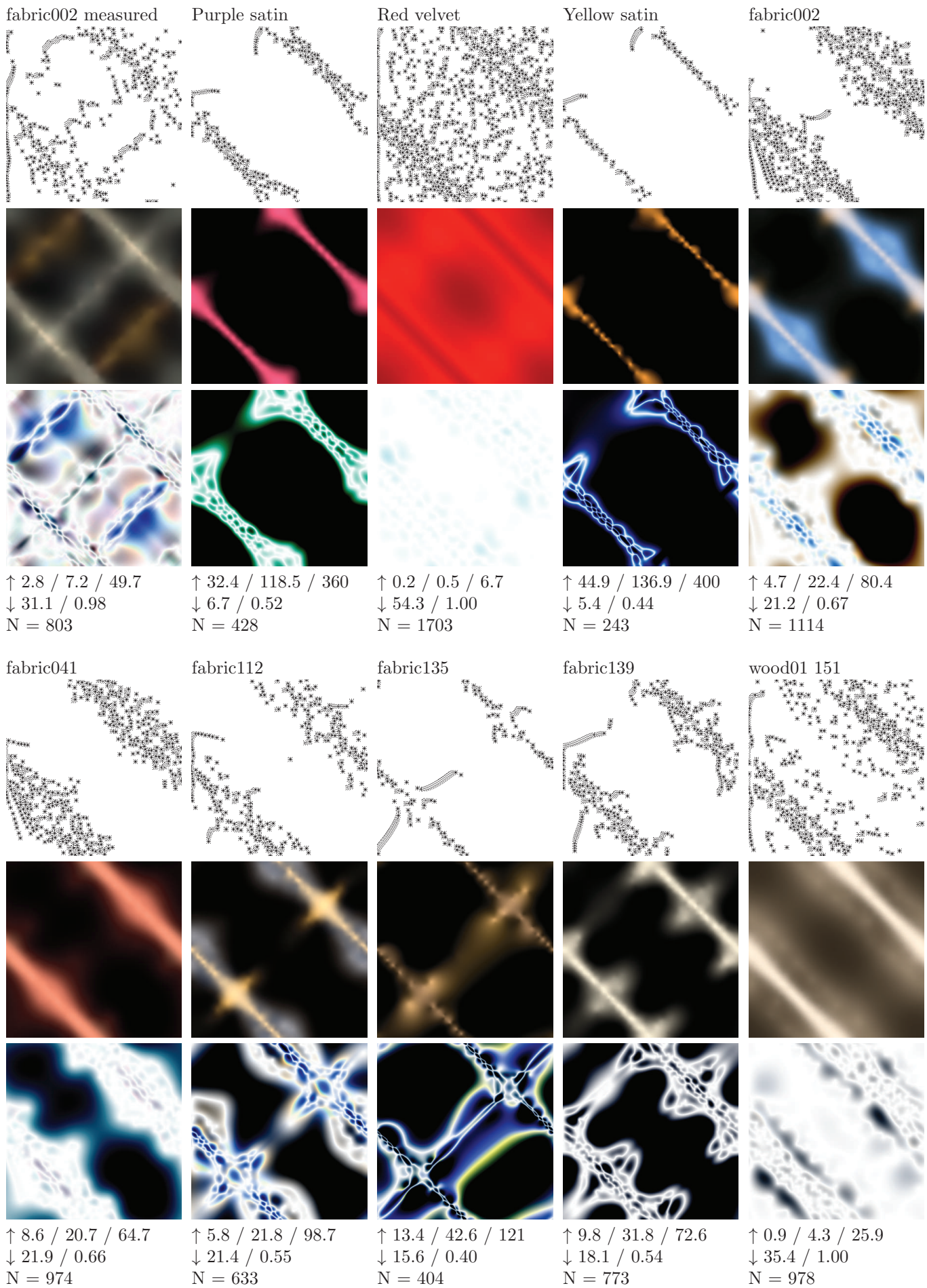


Figure 34: Floyd-Steinberg dithering tested on various materials.

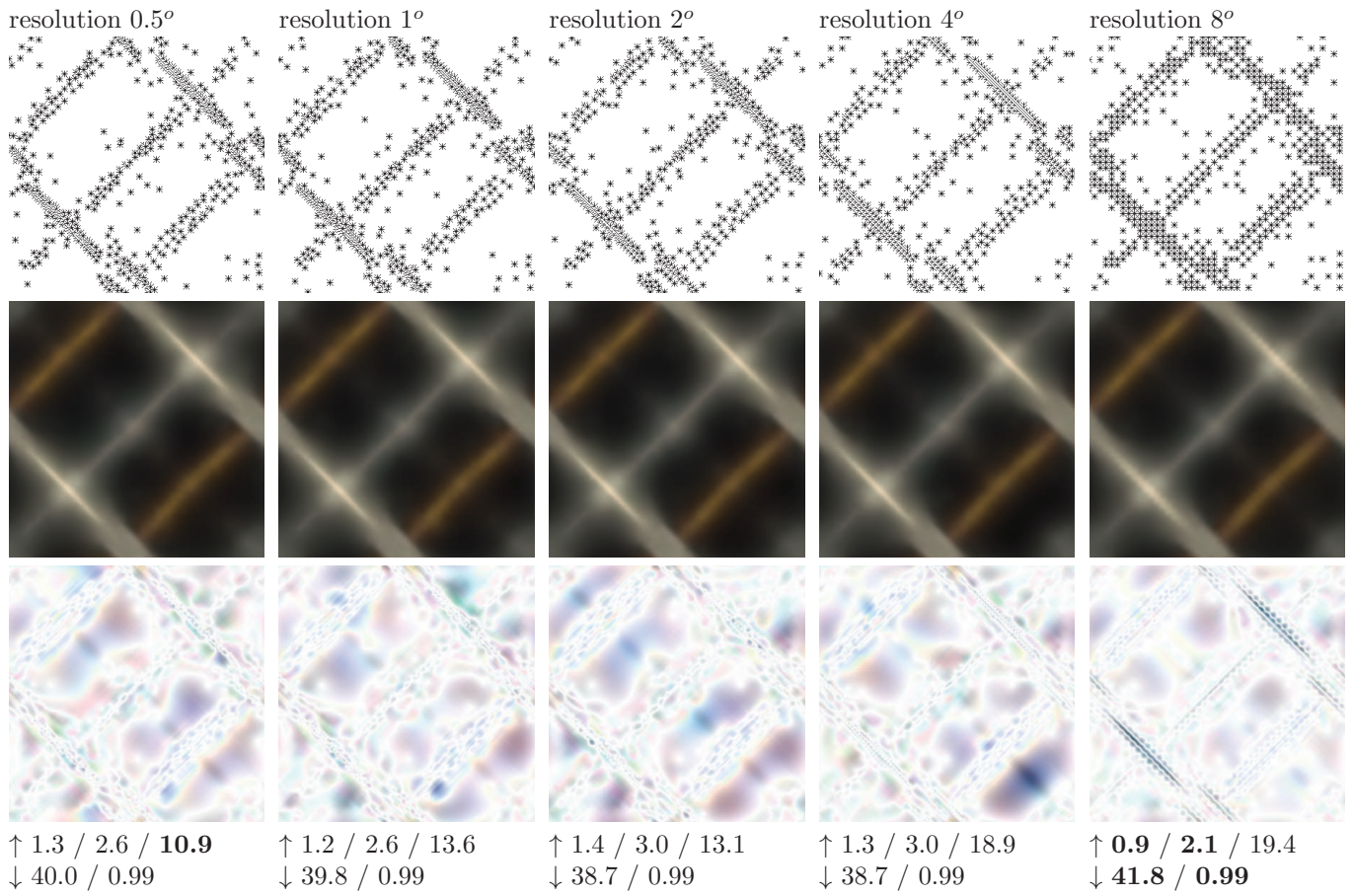


Figure 35: Iterative sample removing with final sample count $N = 576$. Material fabric002 measured.

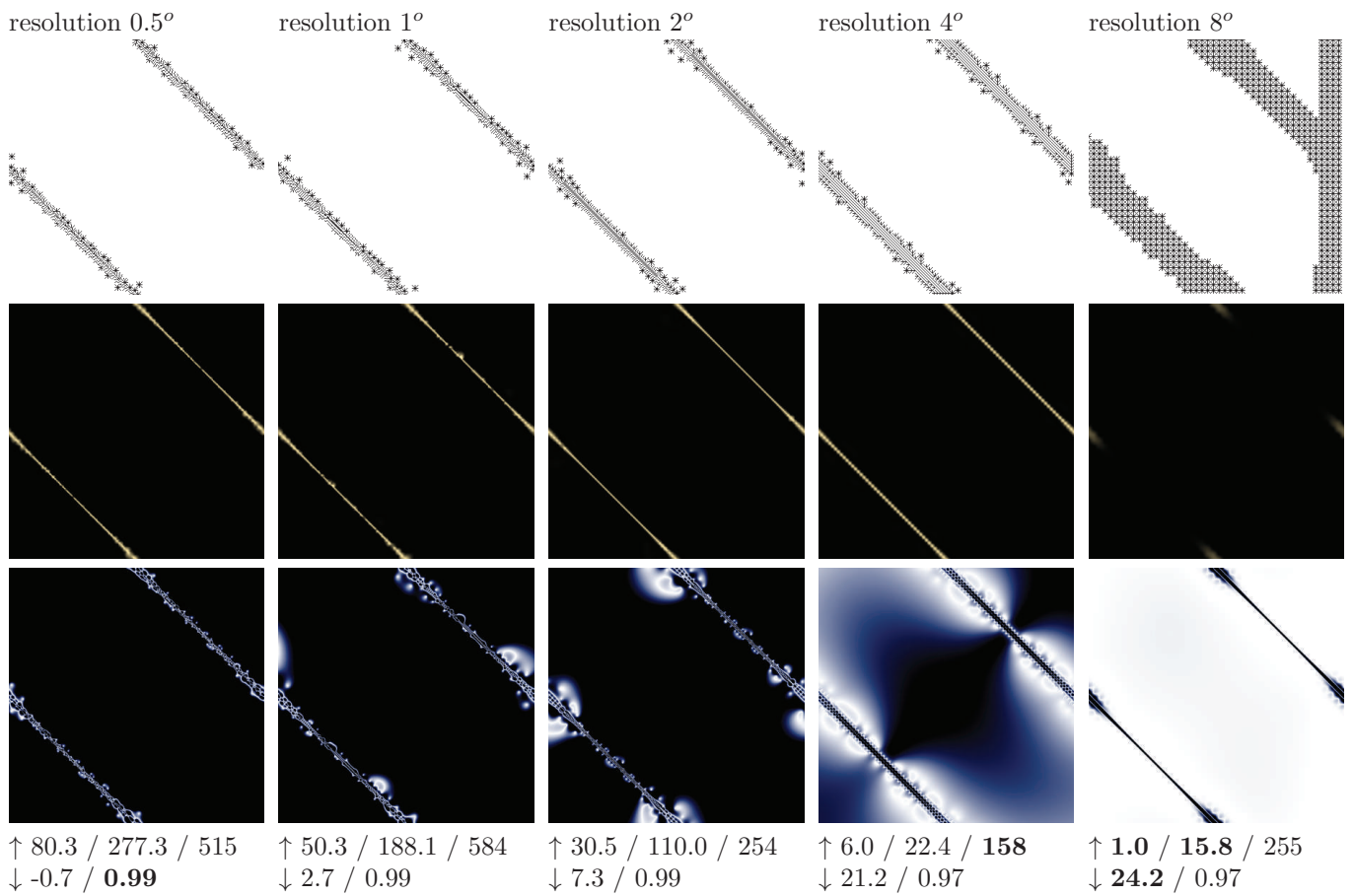


Figure 36: Iterative sample removing with final sample count $N = 576$. Material Brushed alum.

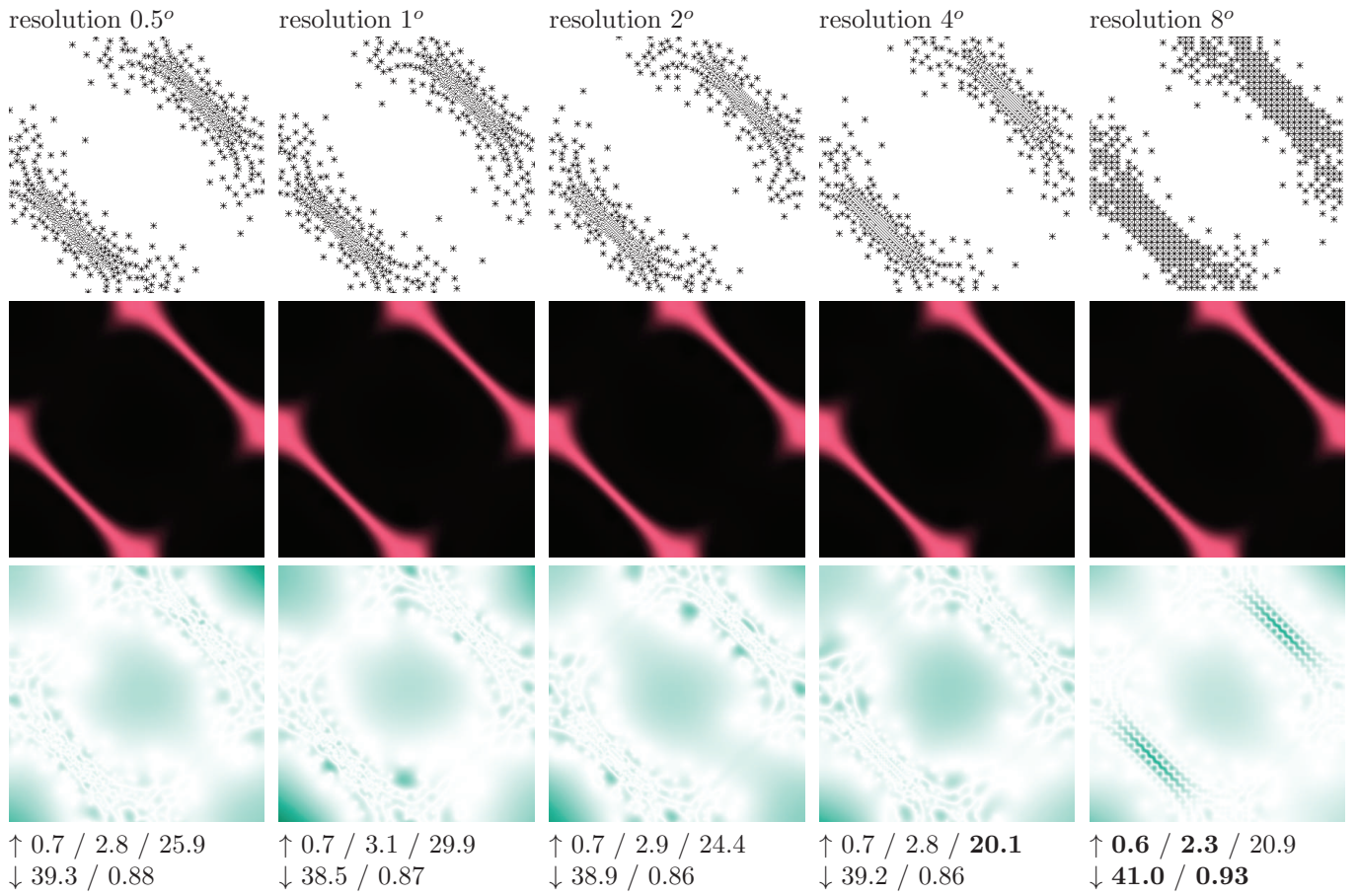


Figure 37: Iterative sample removing with final sample count $N = 576$. Material Purple satin.

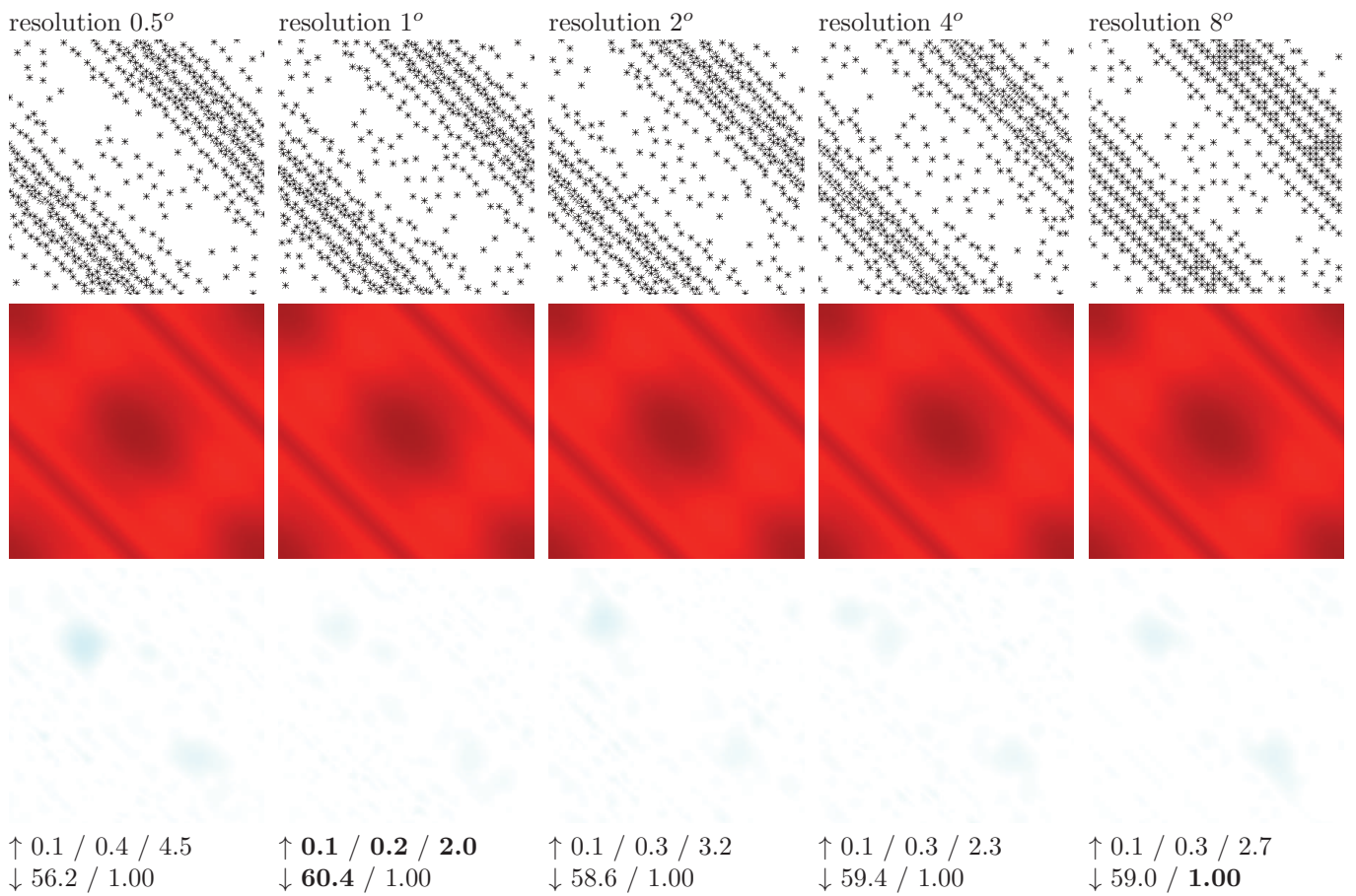


Figure 38: Iterative sample removing with final sample count $N = 576$. Material Red velvet.

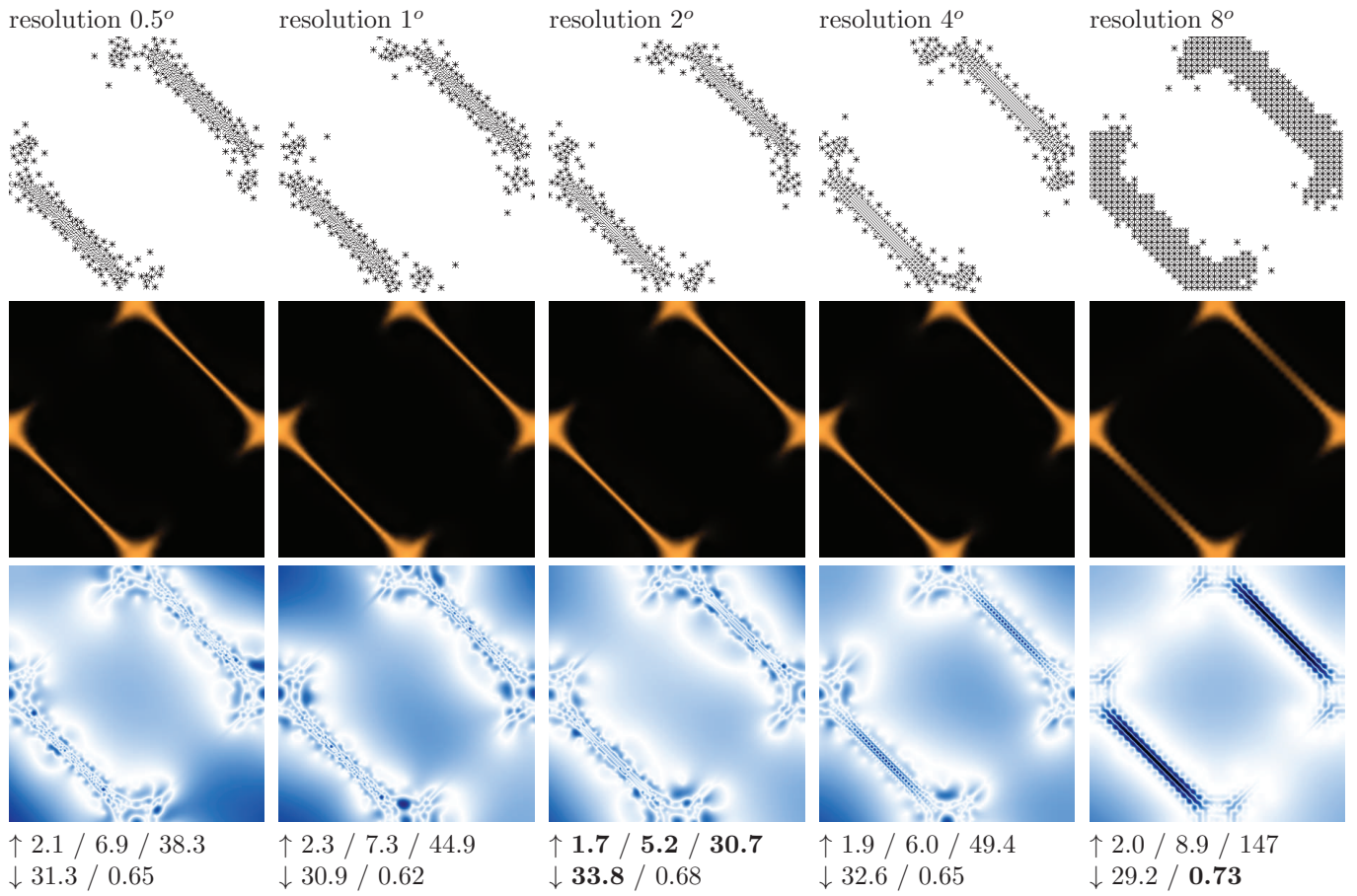


Figure 39: Iterative sample removing with final sample count $N = 576$. Material Yellow satin.

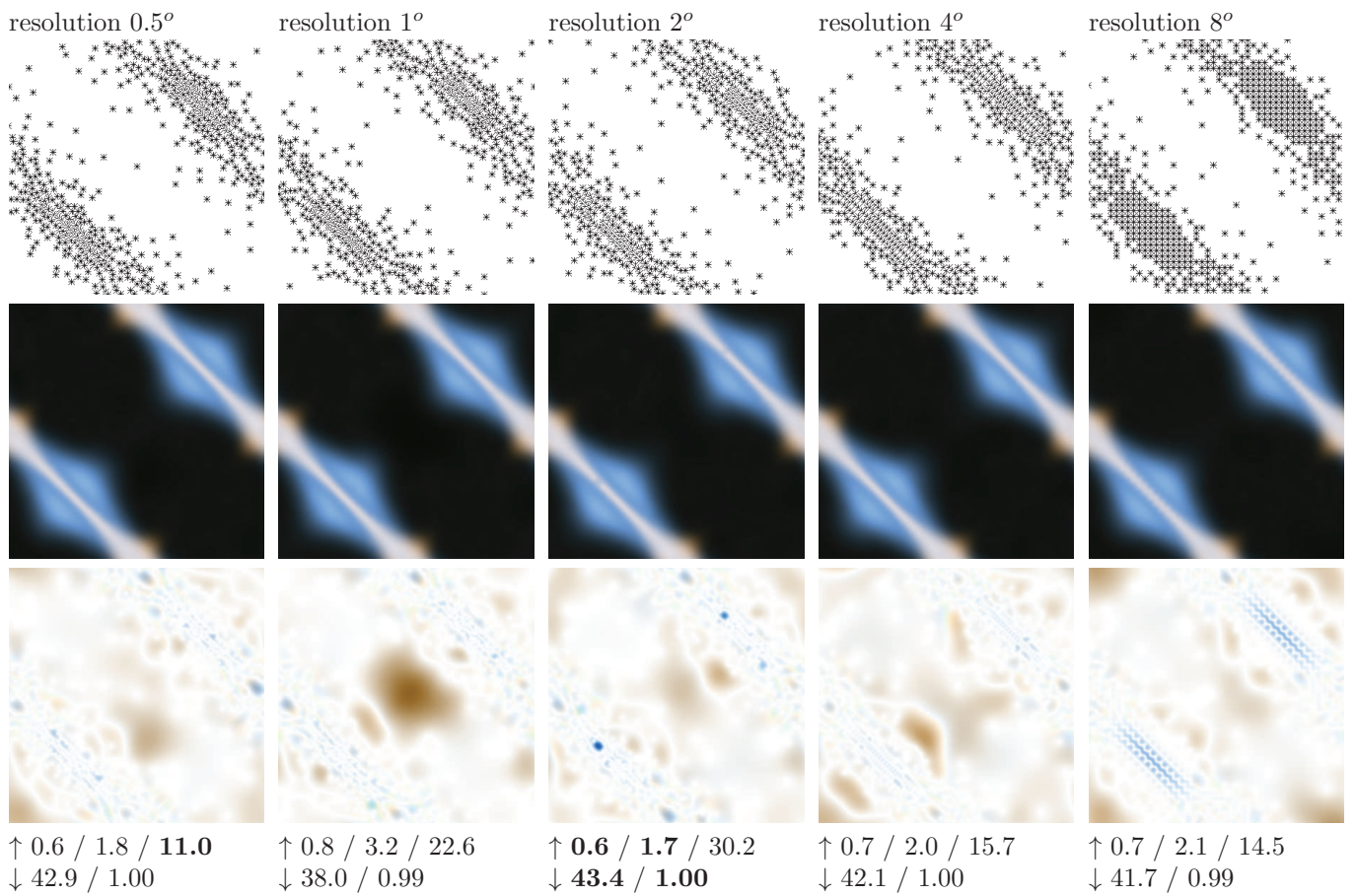


Figure 40: Iterative sample removing with final sample count $N = 576$. Material fabric002.

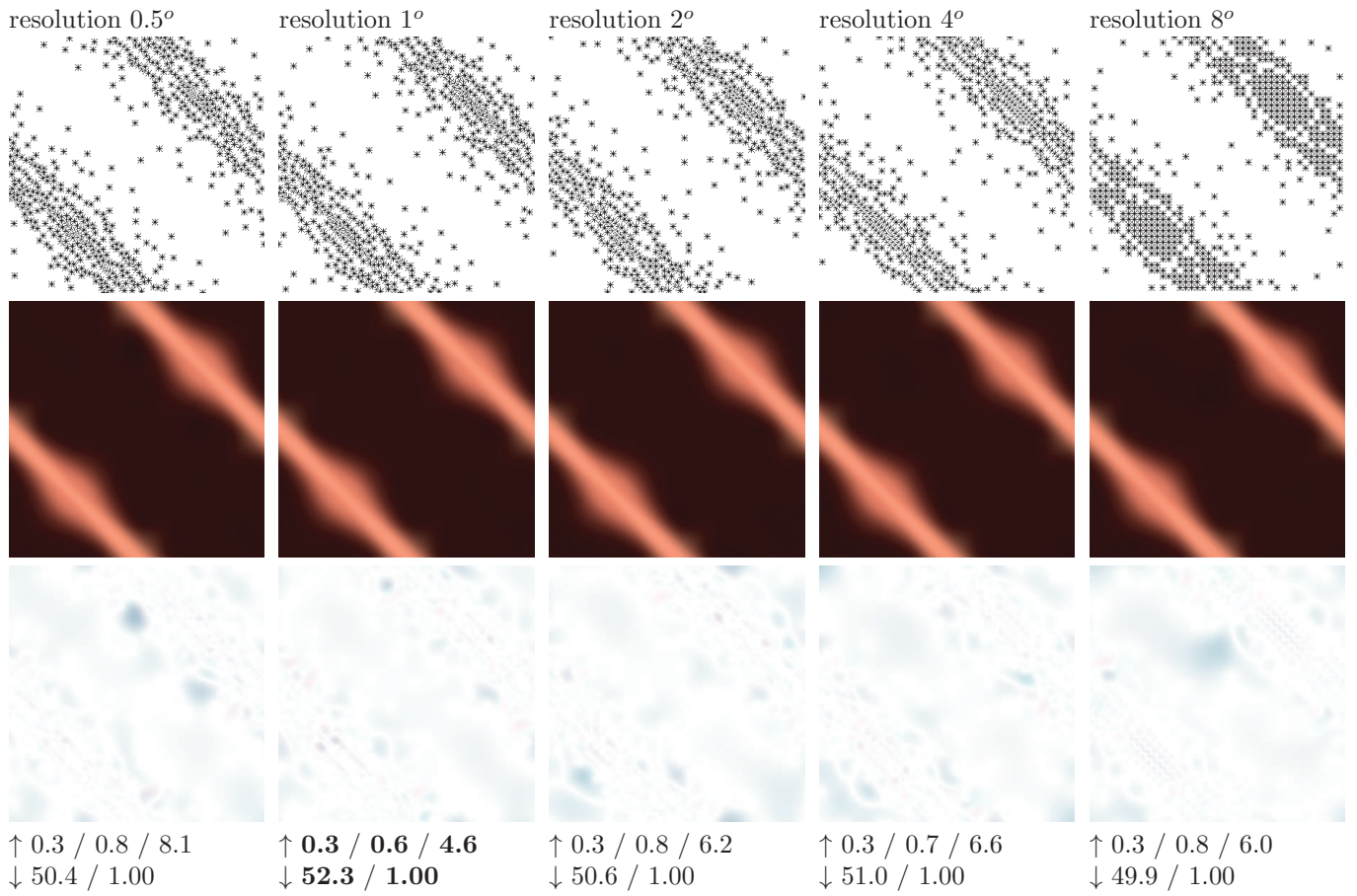


Figure 41: Iterative sample removing with final sample count $N = 576$. Material fabric041.

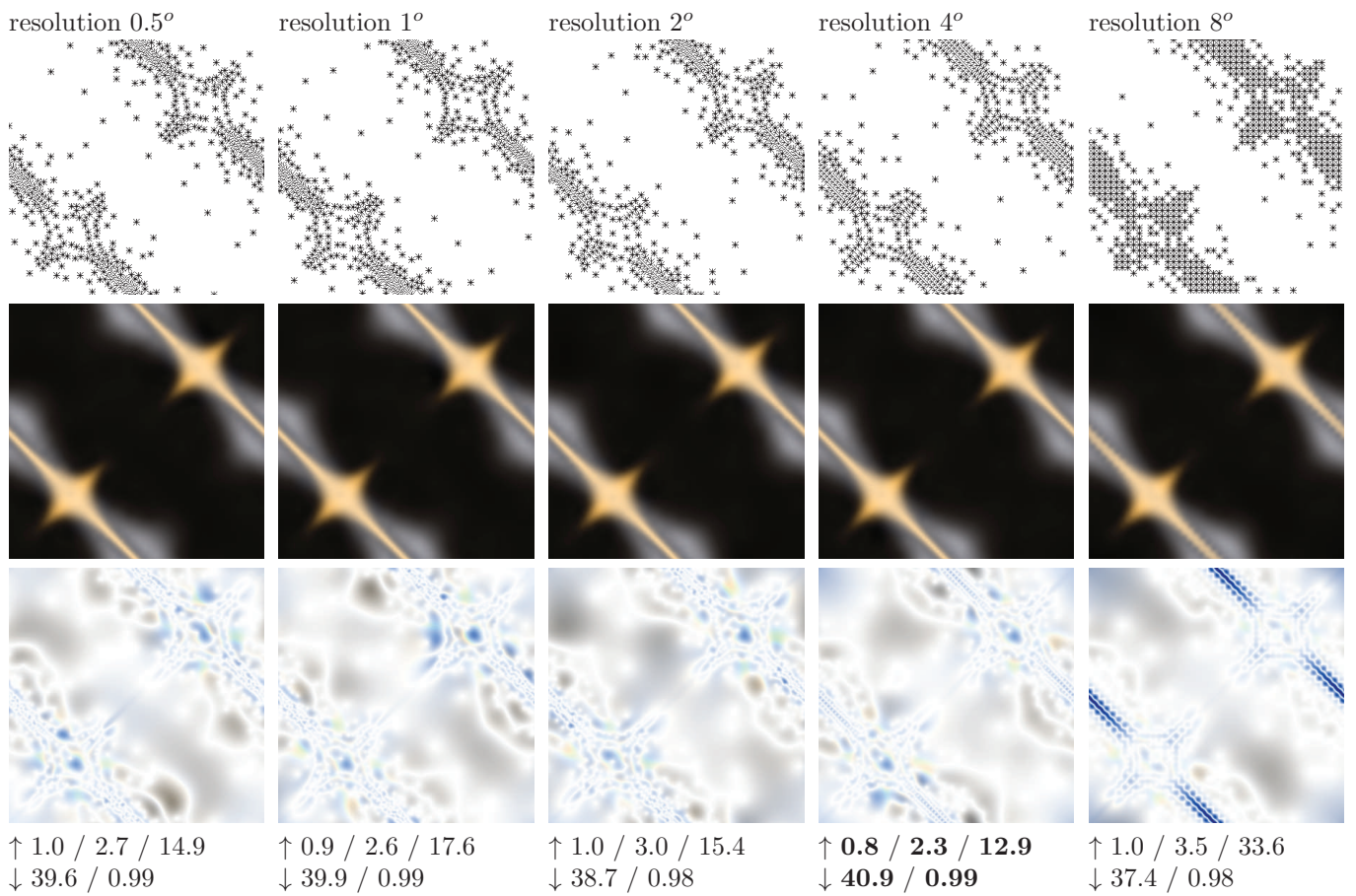


Figure 42: Iterative sample removing with final sample count $N = 576$. Material fabric112.

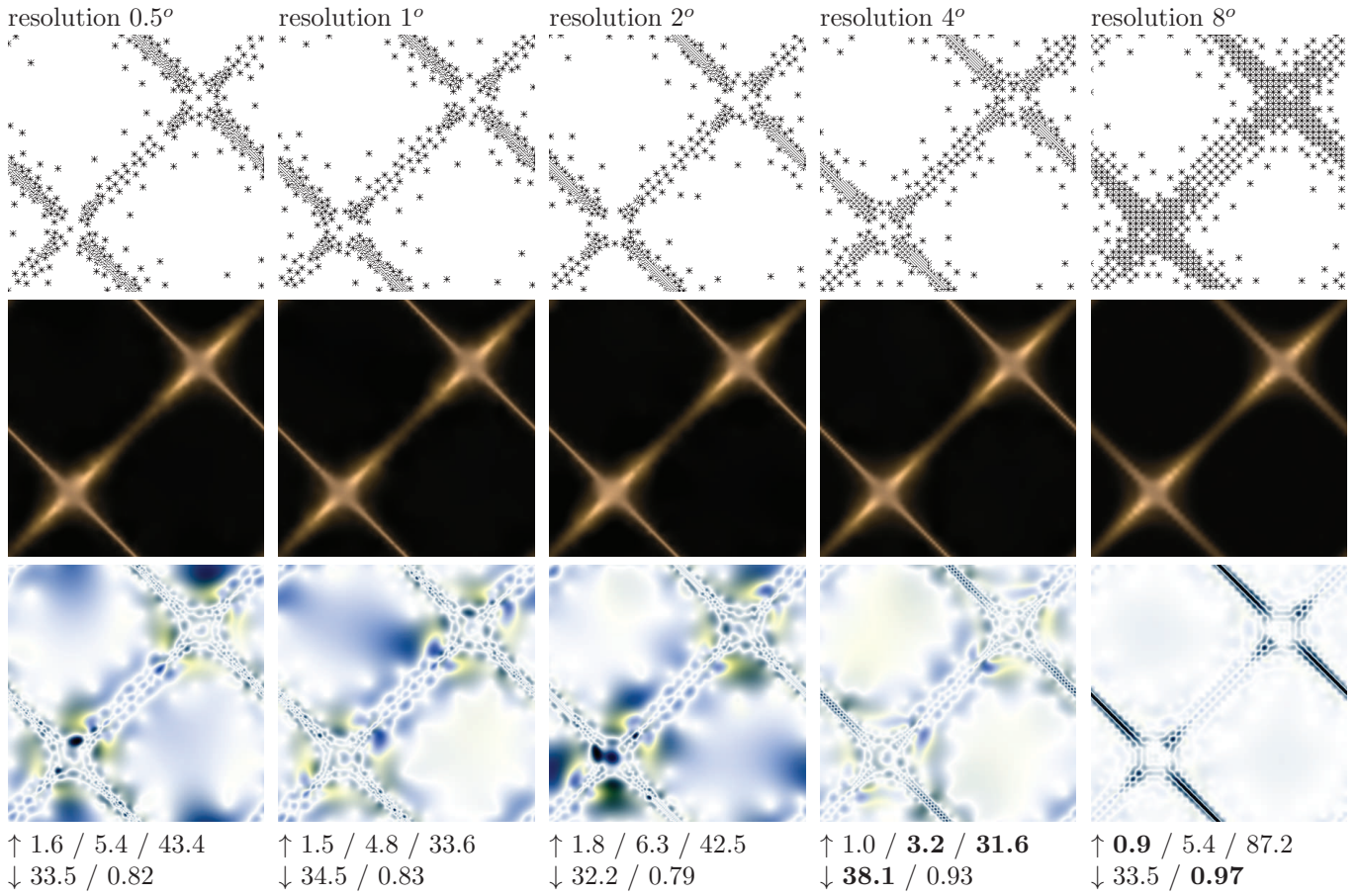


Figure 43: Iterative sample removing with final sample count $N = 576$. Material fabric135.

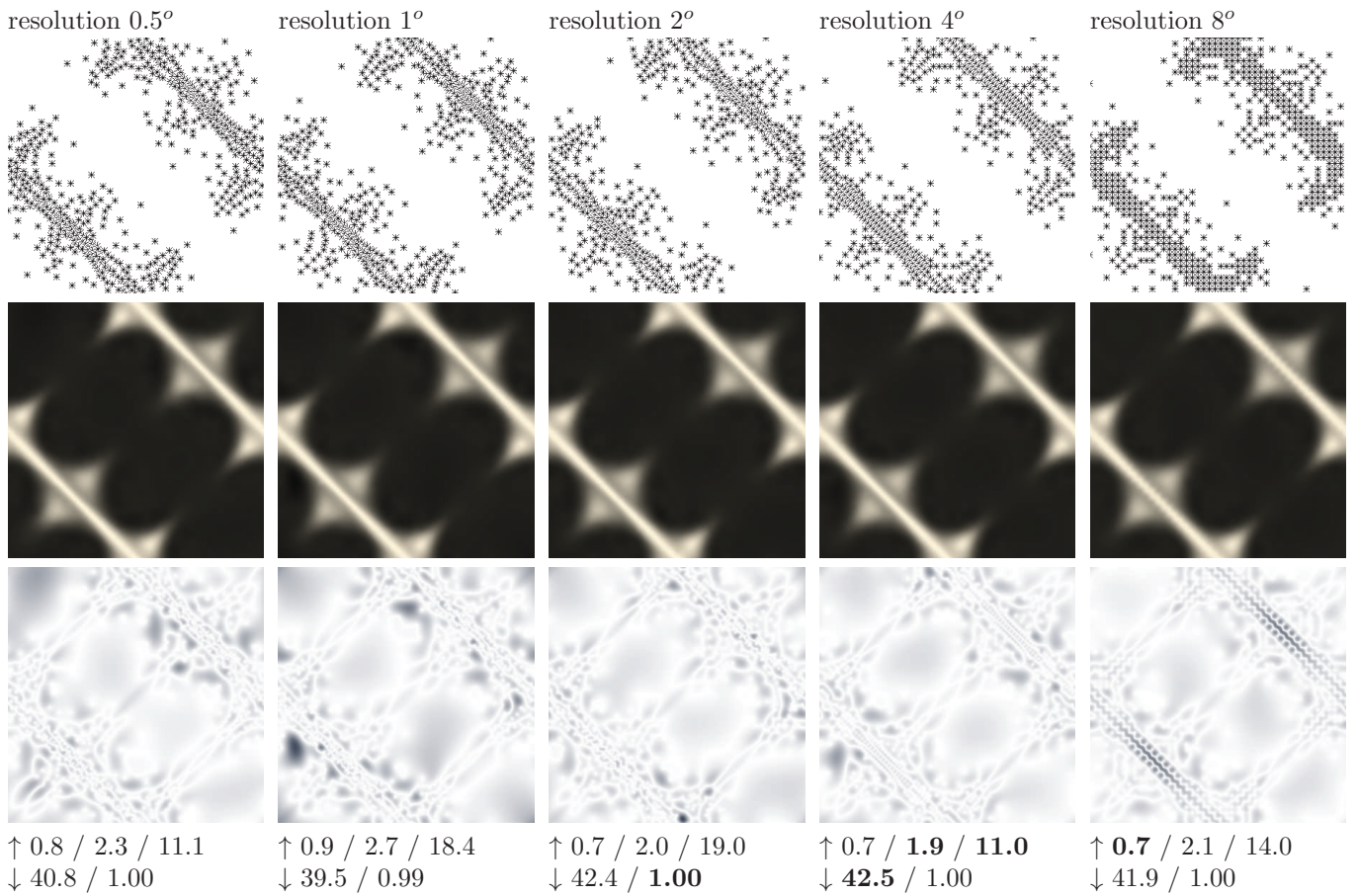


Figure 44: Iterative sample removing with final sample count $N = 576$. Material fabric139.

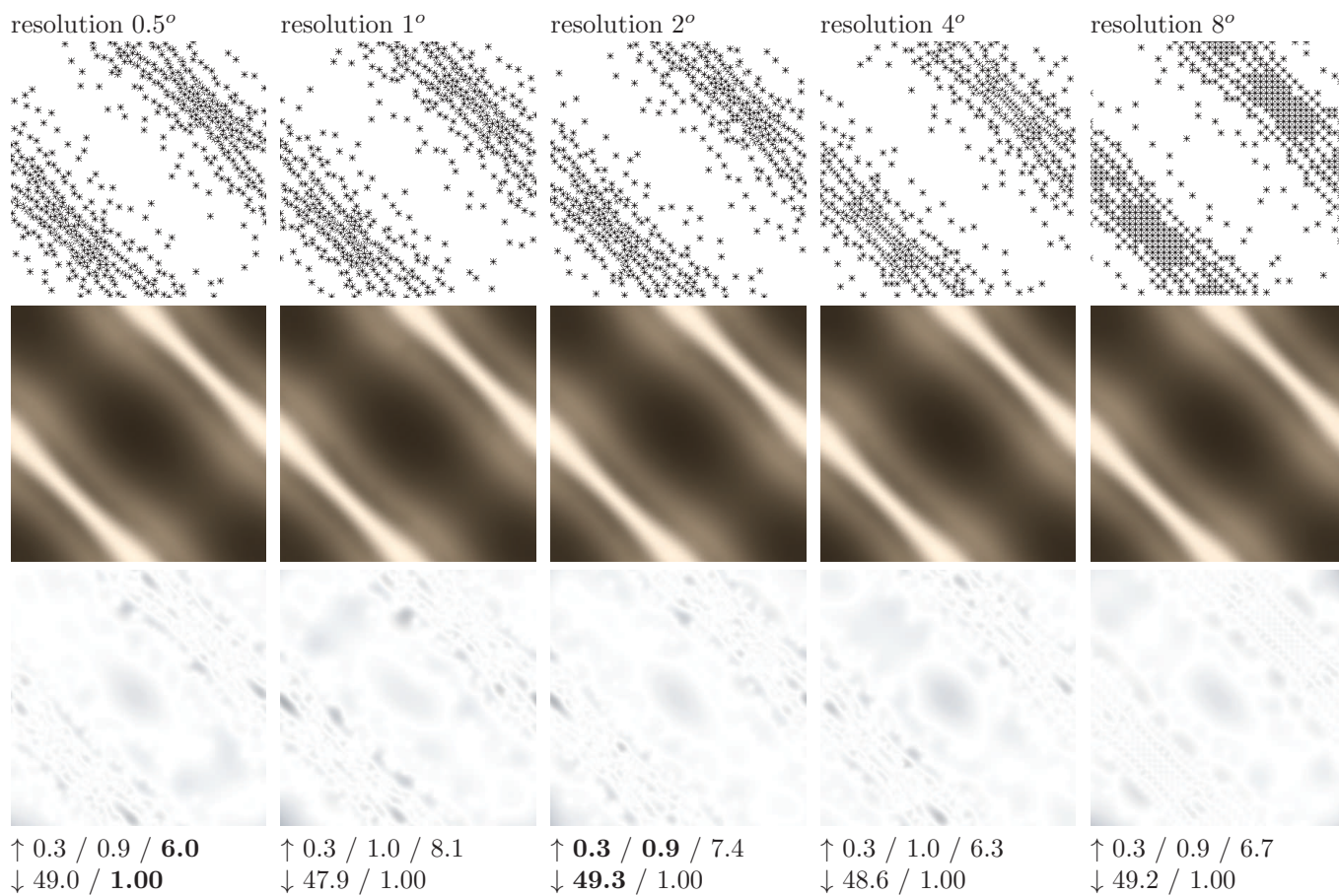


Figure 45: Iterative sample removing with final sample count $N = 576$. Material wood01 151.

6 Final Comparison

For final comparison of the above described methods we selected the algorithm based on iterative sample removing with initial step 4° as it performs better than the other initial steps for the most materials. Further we selected static sampling pattern with uniform grid of resolution 24×24 samples and then we selected two strategies of adaptive sampling. It is strategy 2 and strategy 11 as they perform better than the others.

Iterative sample removing algorithm works well in terms of pixel-wise comparison and maximal difference measure. Regular uniform pattern provide good performance in terms of error metrics however direct pixel-wise comparison of interpolated and ground truth image suggests that interpolated image is not accurate enough as reflections are not smooth.

At least one of the adaptive strategies performs well on the most of materials which suggests that adaptive sampling is possible although it should be improved slightly in the future to compete even better with static regular sampling.

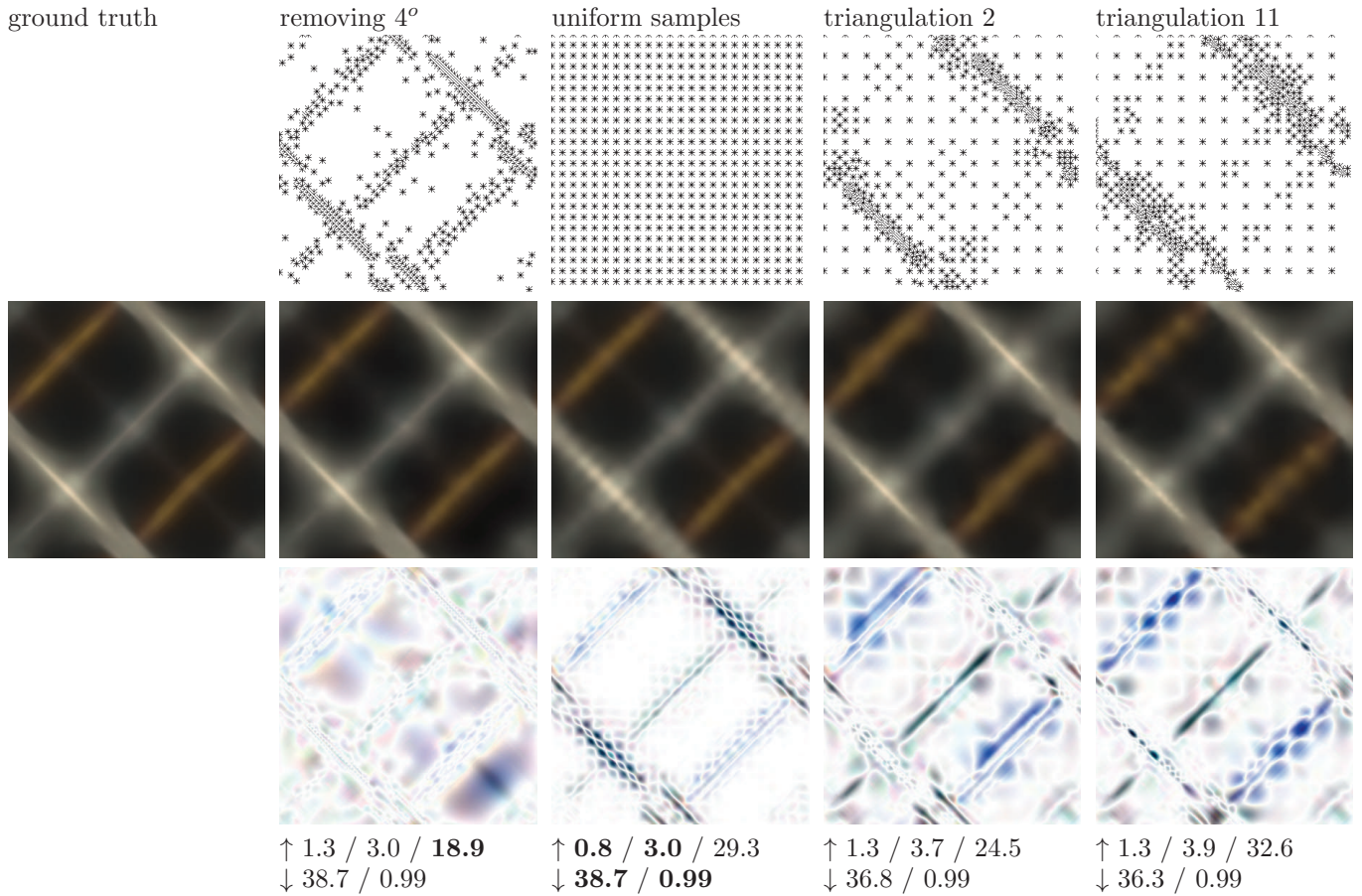


Figure 46: Material fabric002 measured. Sample count $N = 576$.

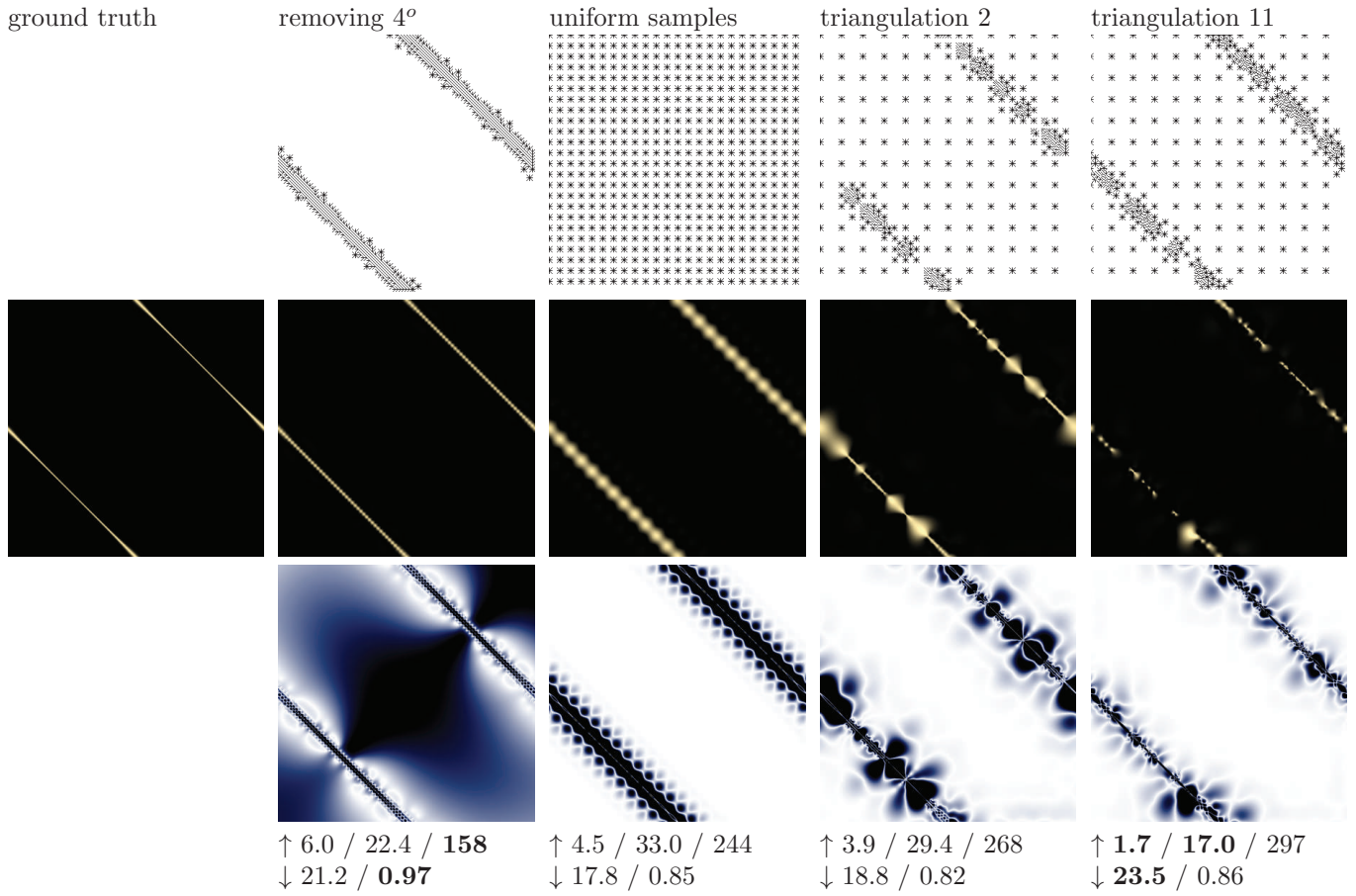


Figure 47: Material Brushed alum. Sample count $N = 576$.

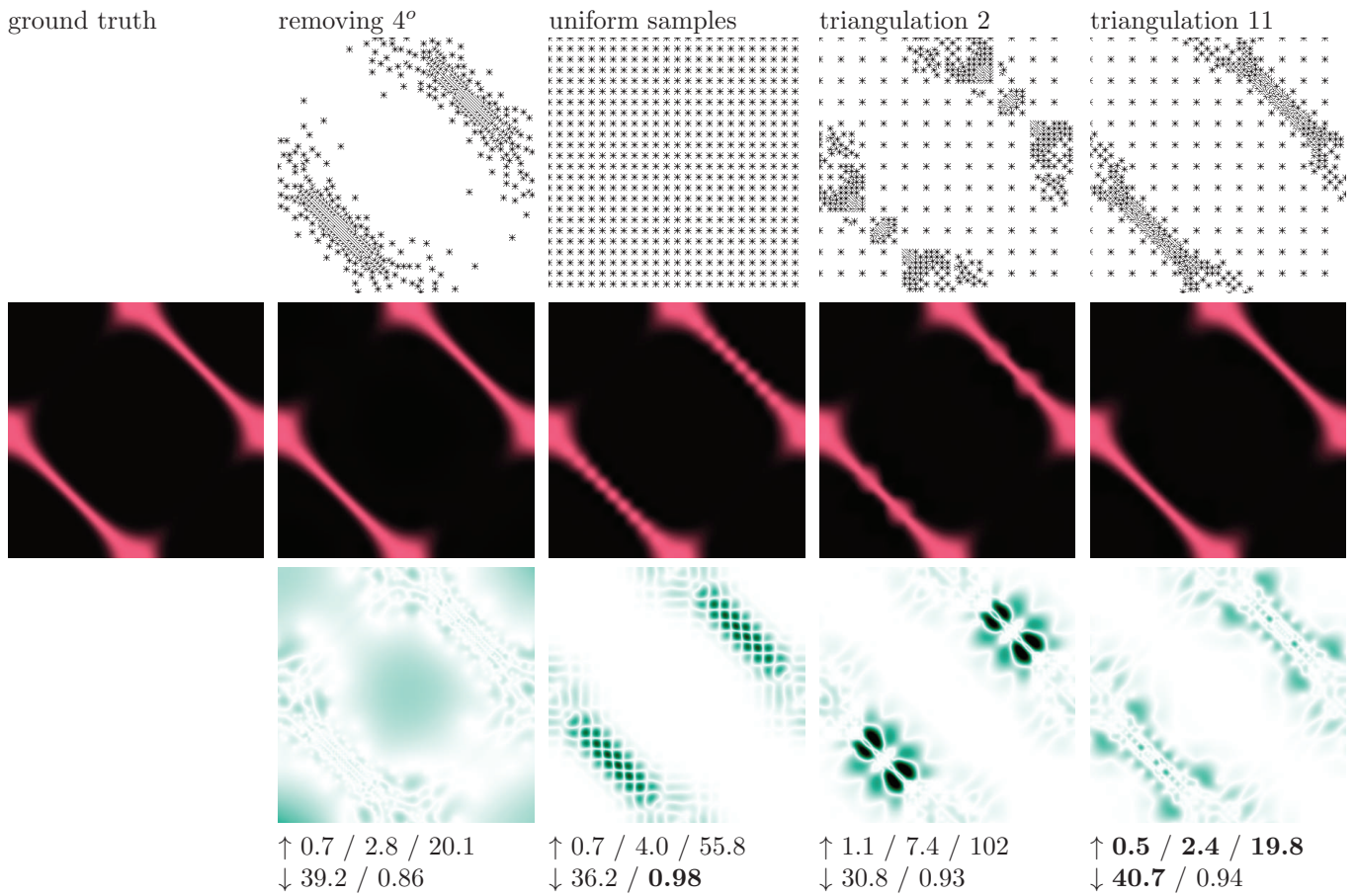


Figure 48: Material Purple satin. Sample count $N = 576$.

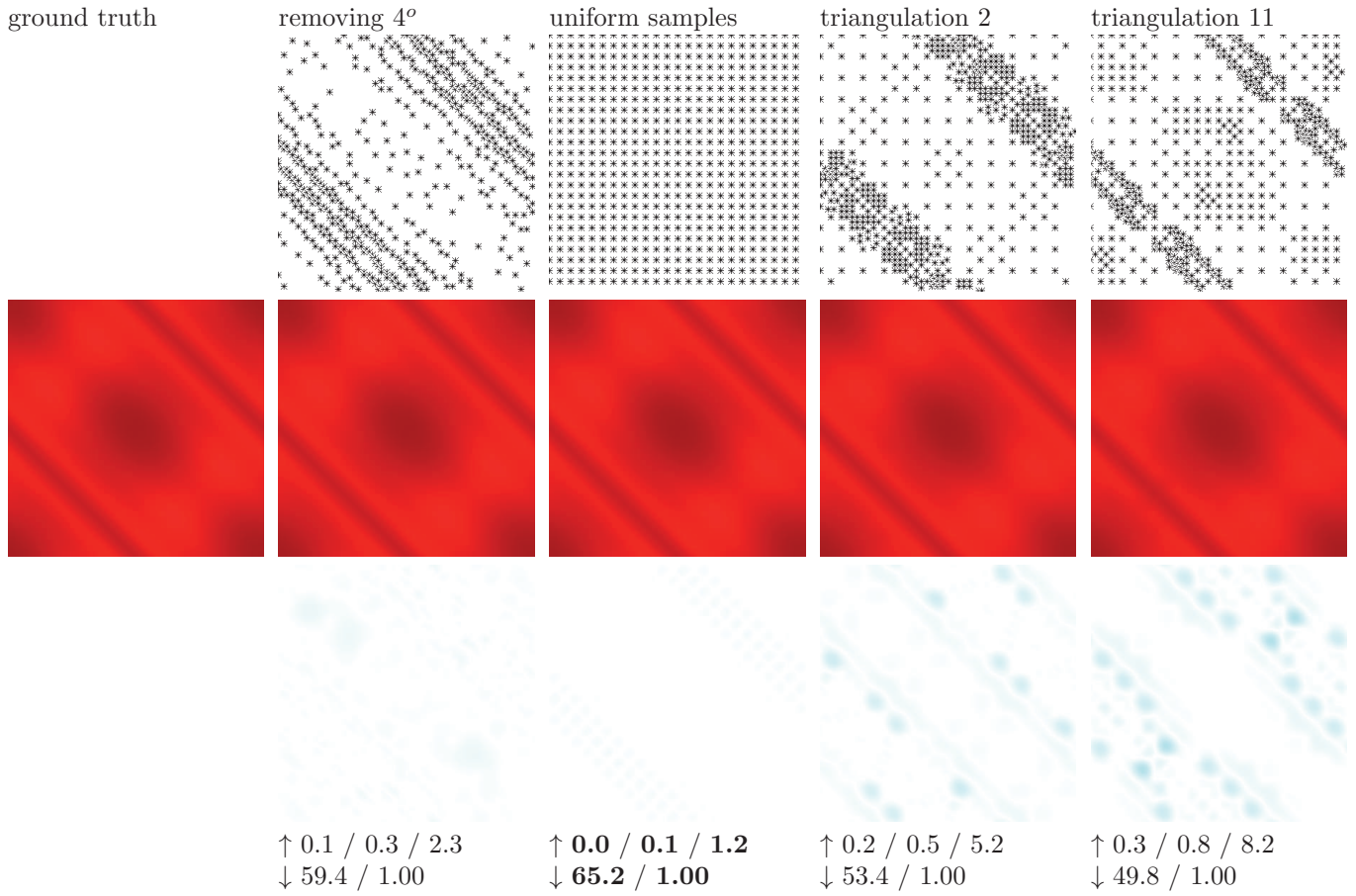


Figure 49: Material Red velvet. Sample count $N = 576$.

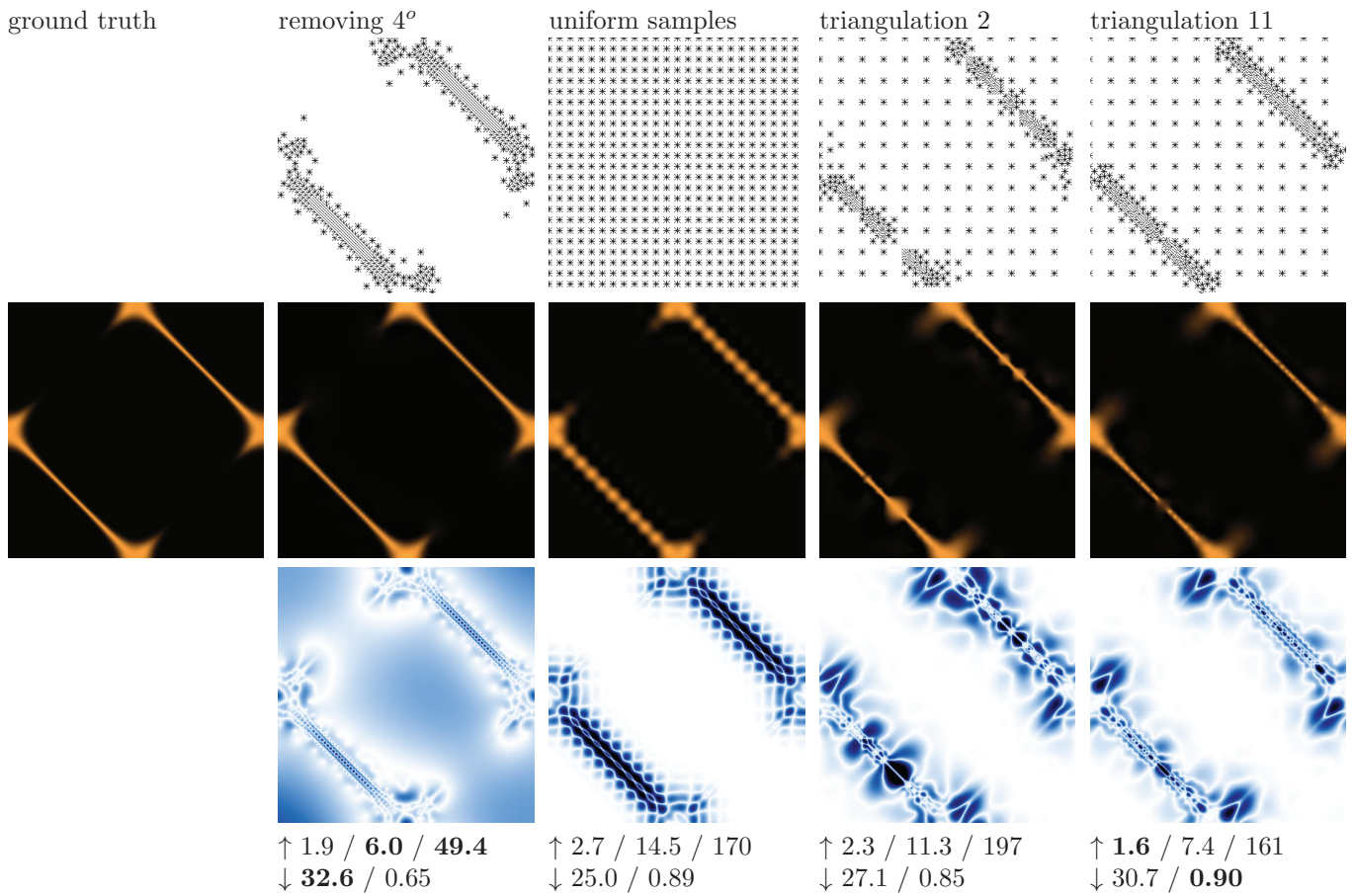


Figure 50: Material Yellow satin. Sample count $N = 576$.

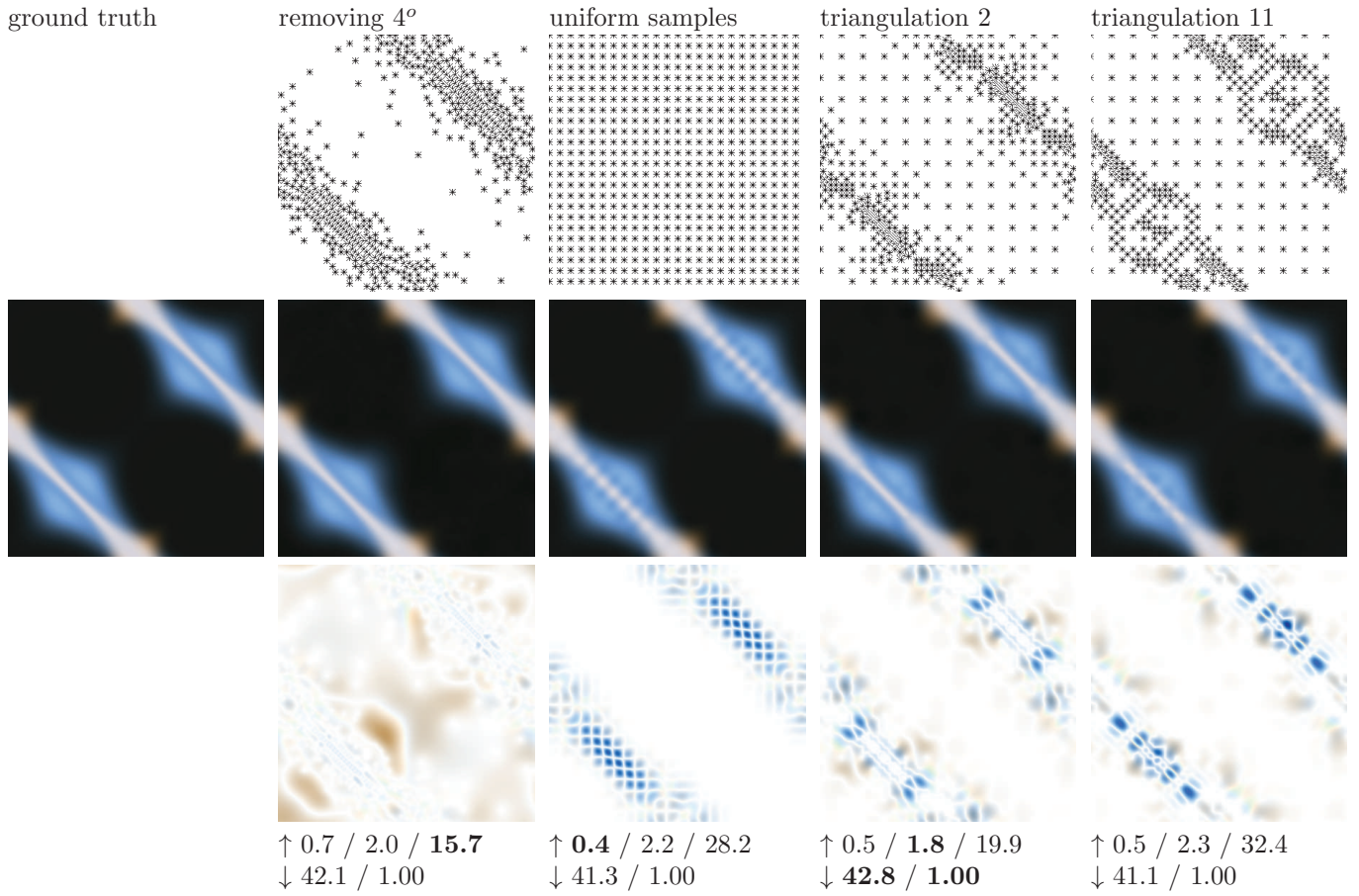


Figure 51: Material fabric002. Sample count $N = 576$.

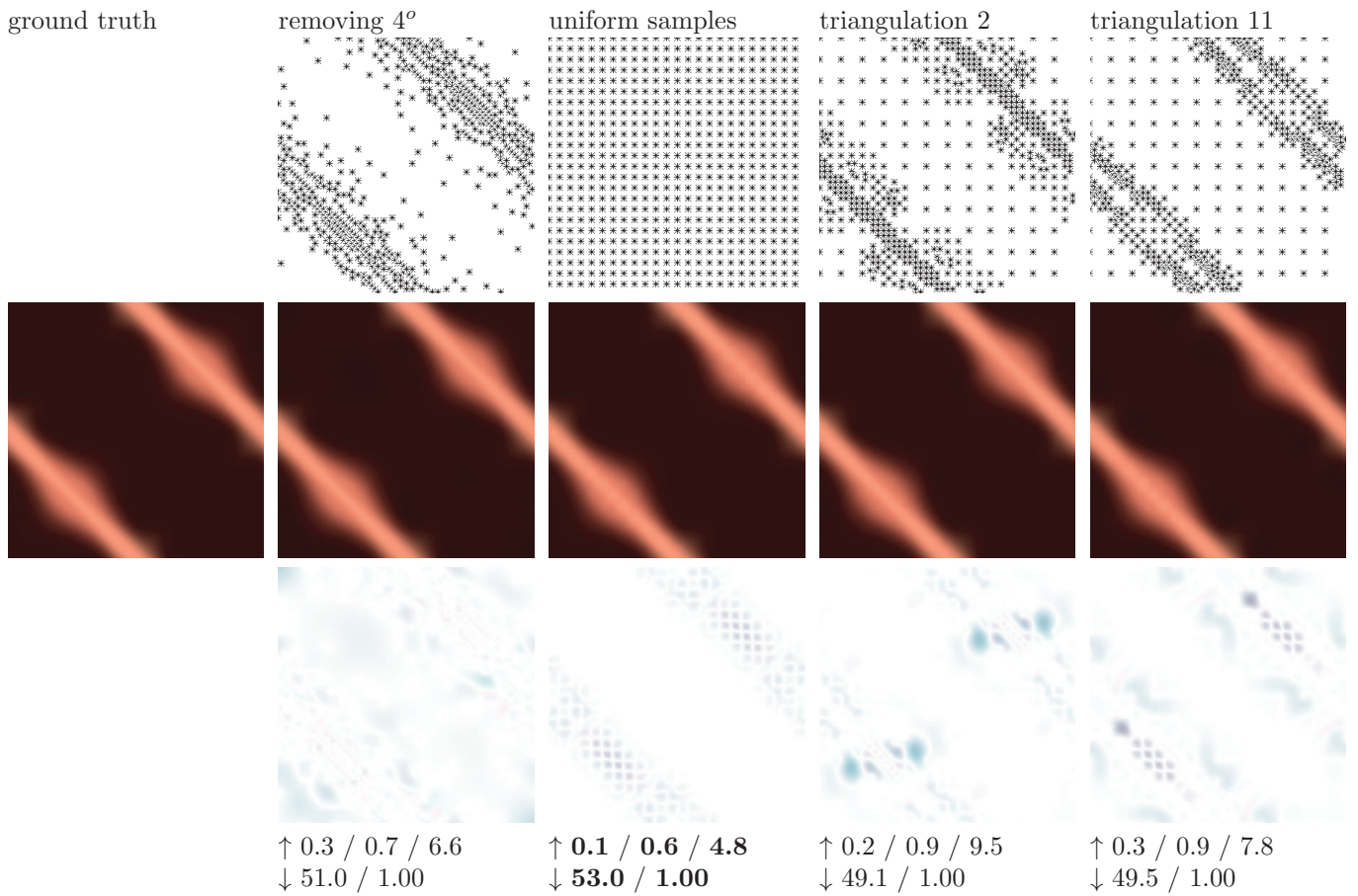


Figure 52: Material fabric041. Sample count $N = 576$.

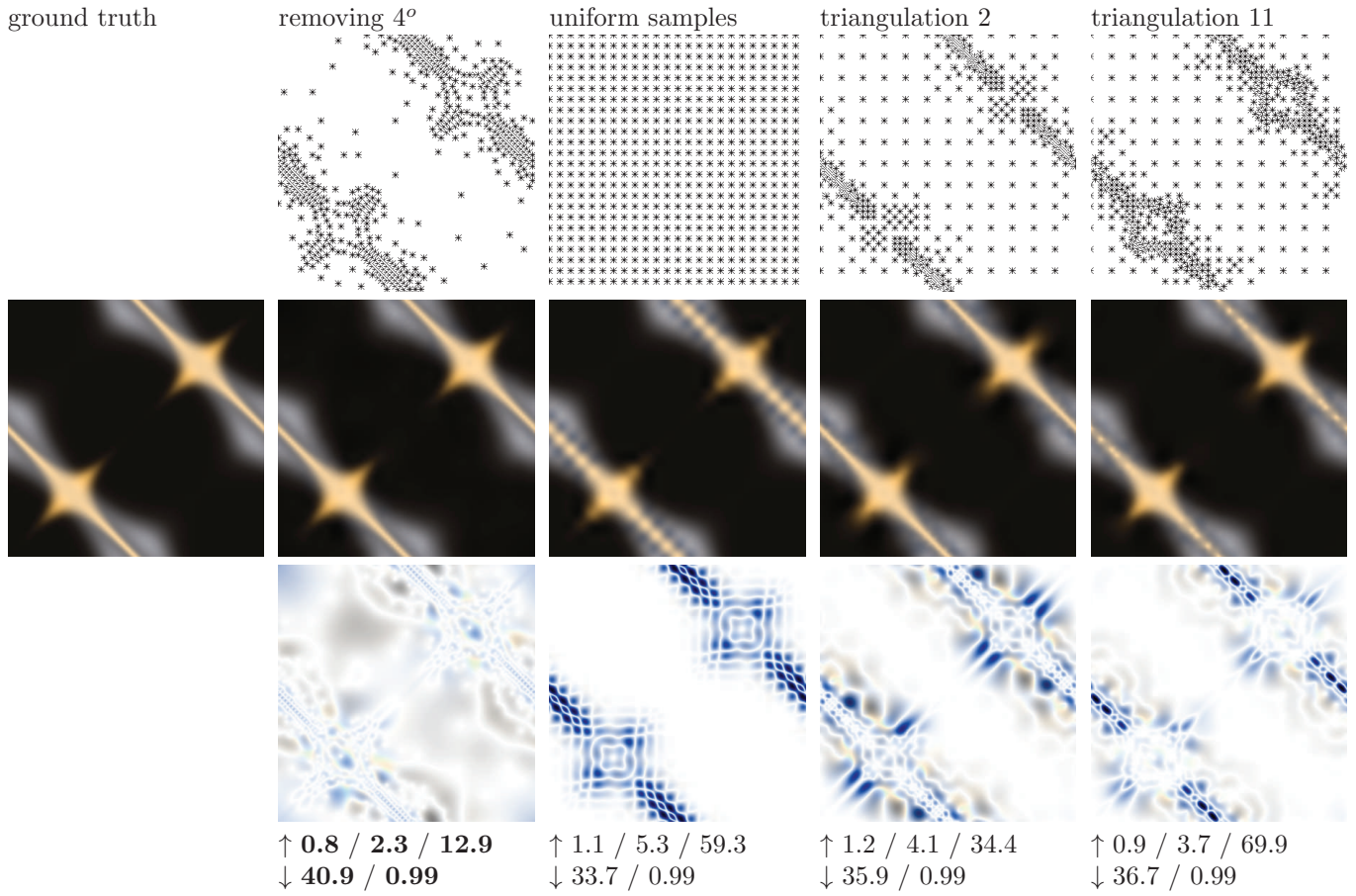


Figure 53: Material fabric112. Sample count $N = 576$.

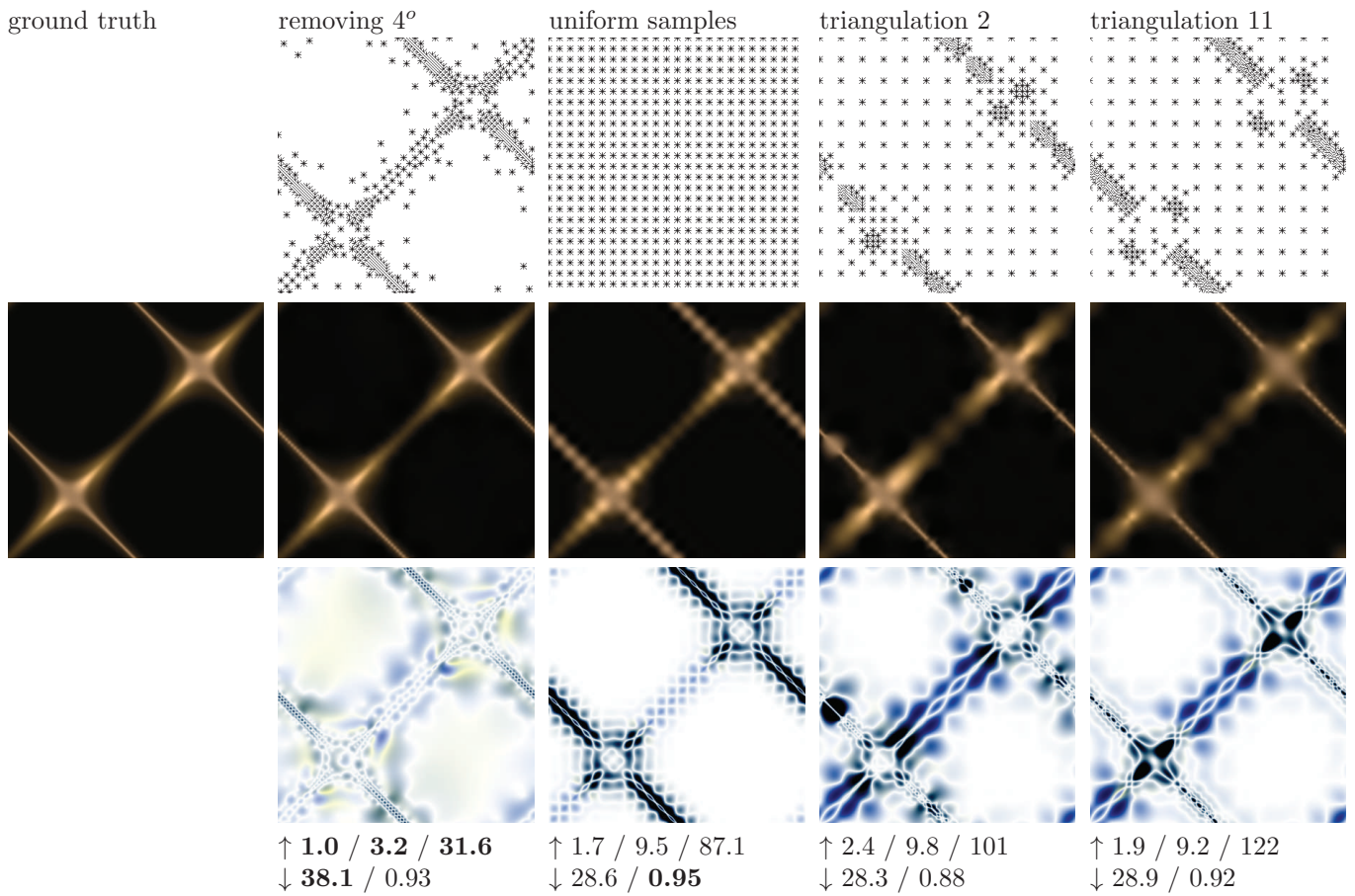


Figure 54: Material fabric135. Sample count $N = 576$.

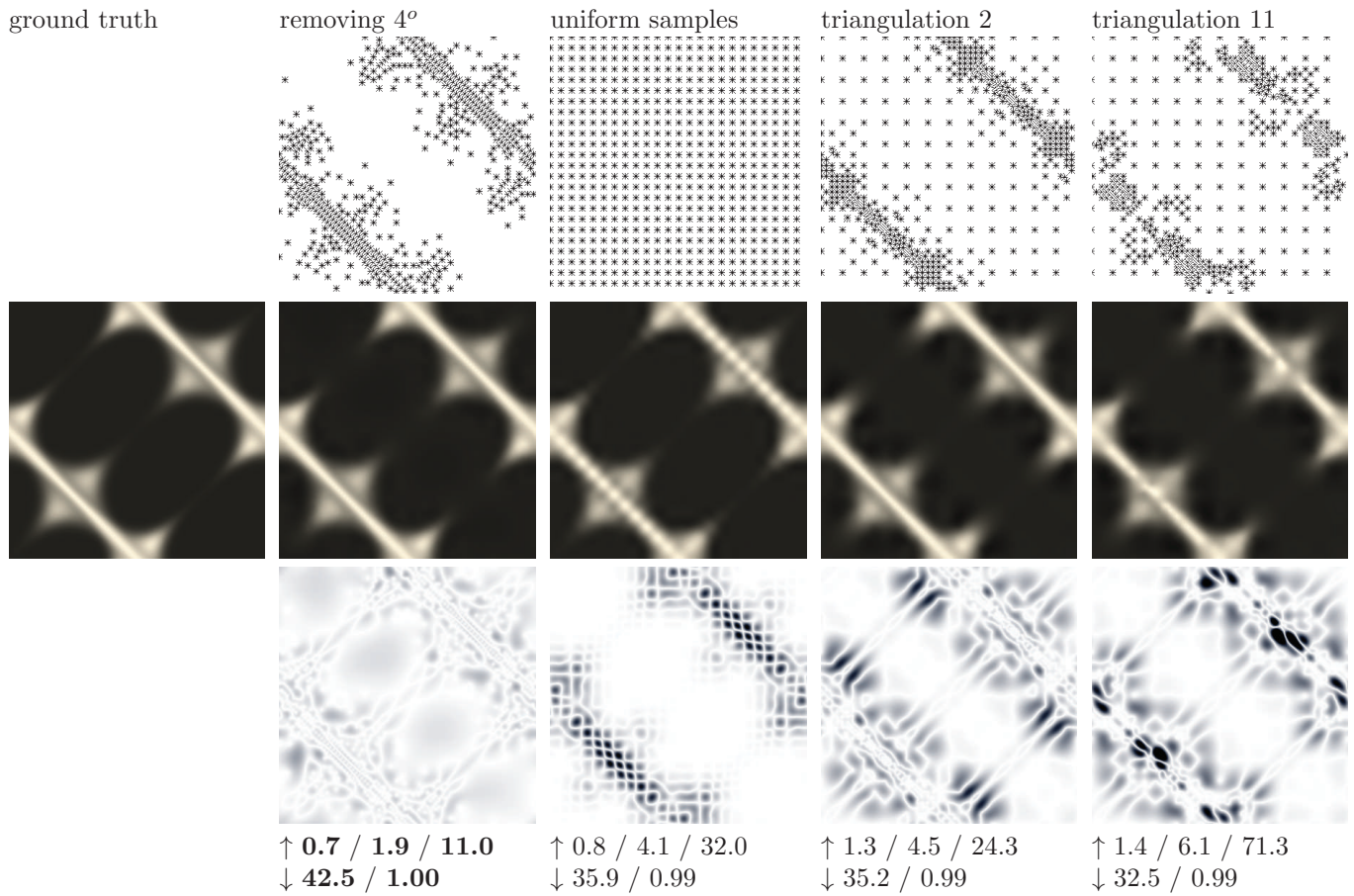


Figure 55: Material fabric139. Sample count N = 576.

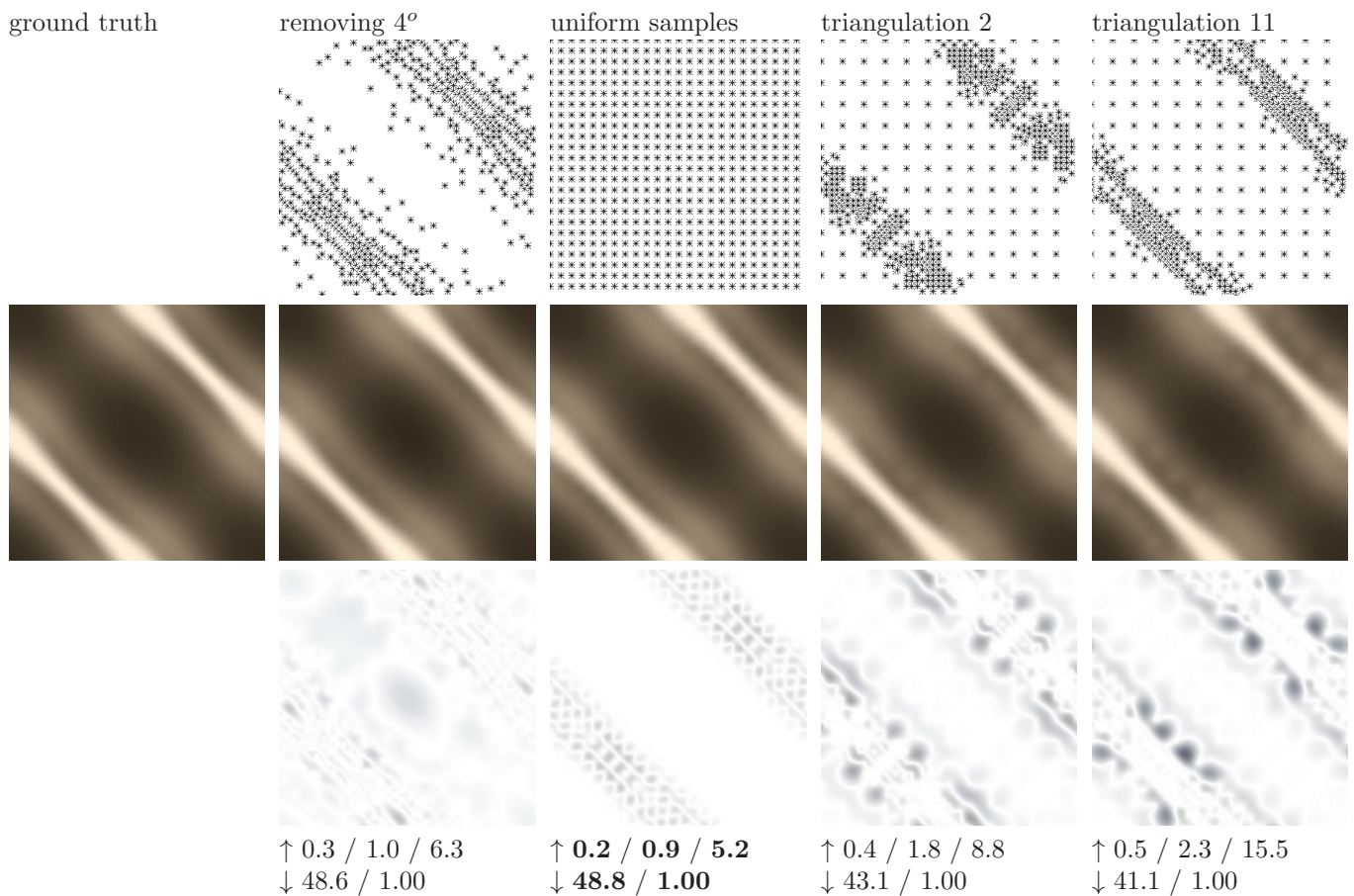


Figure 56: Material wood01 151. Sample count N = 576.

References

- [1] H. S. M. Coxeter. *Introduction to Geometry*. New York: Wiley, 1969.
- [2] J. Filip, R. Vavra, M. Haindl, P. Zid, M. Krupicka, and V. Havran. BRDF slices: Accurate adaptive anisotropic appearance acquisition. In *CVPR 2013*, pages 4321–4326, 2013.
- [3] Robert W. Floyd and Louis Steinberg. An Adaptive Algorithm for Spatial Greyscale. *Proceedings of the Society for Information Display*, 17(2):75–77, 1976.
- [4] Martin Fuchs, Volker Blanz, Hendrik P.A. Lensch, and Hans-Peter Seidel. Adaptive sampling of reflectance fields. *ACM Trans. Graph.*, 26(2):1–18, June 2007.
- [5] Steven J. Gortler, Radek Grzeszczuk, Richard Szeliski, and Michael F. Cohen. The lumigraph. In *SIGGRAPH '96*, pages 43–54, 1996.
- [6] M. Kurt, L. Szirmay-Kalos, and J. Krivánek. An anisotropic BRDF model for fitting and Monte Carlo rendering. *SIGGRAPH Comput. Graph.*, 44:3:1–3:15, February 2010.
- [7] A. Ngan, F. Durand, and W. Matusik. Experimental analysis of BRDF models. *Eurographics Symposium on Rendering 2005*, 2:117–126, 2005.
- [8] F.E. Nicodemus, J.C. Richmond, J.J. Hsia, I.W. Ginsburg, and T. Limperis. Geometrical considerations and nomenclature for reflectance. *NBS Monograph 160, National Bureau of Standards, U.S. Dept. of Com.*, pages 1–52, 1977.
- [9] W. H. Press, S. A. Teukolsky, William T. Vetterling, and Brian P. Flannery. *Numerical Recipes in C: The Art of Scientific Computing*. Cambridge University Press, 1992.
- [10] Zhou Wang, A.C. Bovik, H.R. Sheikh, and E.P. Simoncelli. Image quality assessment: from error visibility to structural similarity. *Image Processing, IEEE Transactions on*, 13(4):600–612, 2004.

Acknowledgments

This research has been supported by the Czech Science Foundation grant 103/11/0335.